Habib Zambrano

Fatigue Assessment of Notches and Cracks in Ductile Cast Iron

Thesis for the degree of Philosophiae Doctor

Trondheim, September 2011

Norwegian University of Science and Technology
Faculty of Engineering Science and Technology
Department of Engineering Design and Materials

NTNU – Trondheim
Norwegian University of
Science and Technology

NTNU
Norwegian University of Science and Technology

Thesis for the degree of Philosophiae Doctor

Faculty of Engineering Science and Technology
Department of Engineering Design and Materials

ISBN 978-82-471-3006-3 (printed ver.)
ISBN 978-82-471-3007-0 (electronic ver.)
ISSN 1503-8181

Doctoral theses at NTNU, 2011:224

Printed by NTNU-trykk

To: ***God****, my wife* ***Beatriz*** *and my son* ***Juan D****.*

Preface

This doctoral thesis consists of an introduction and four papers. One paper has been accepted for publication, two papers have been submitted for publication in international journals and one will be submitted. The work has been carried out under the supervision of Professor Gunnar Härkegård and in close collaboration with colleagues at NTNU, Alstom Ltd and SP Technical Research Institute of Sweden.

In Paper 1, I am the main author.

In Paper 2, the experiments were carried out by Dr. Klaus Stärk at Alstom Ltd., Switzerland. The data were processed by me and I am the main author and responsible for theory, calculations and algorithms.

In Paper 3, I am the main author and responsible for the experiments.

In Paper 4, the experiments were carried out at SP Technical Research Institute of Sweden. The finite element analysis of the rotating bending specimen was carried out by Mehdi Shirani. The data were processed by me and I am the main author and responsible for theory and calculations.

The financial support has been provided by MATSINT program and the Norwegian Research Council. The experiments in Paper 2 were funded by Alstom Wind, Spain.

Acknowledgement

The present work would have been impossible without the contribution of some colleagues whom I would like to acknowledge.

Firstly, I wish to express my deepest gratitude to my supervisor Professor Gunnar Härkegård for giving me this opportunity and for his inspiration, patience, support and encouragement during whole this work. In addition I would like to thank my co-supervisor PhD Sigmund Kyrre Ås for fruitful discussions.

I would like to acknowledge Professor Stig Berge for obtaining financial support to carry out experiments in the fatigue lab and in addition to extend my stay in the institute.

I would also like to thank Dr. Klaus Stärk for the excellent experimental data that he obtained in the lab at Alstom Ltd.

I would like to thank Dr. Thomas Svensson at SP Technical Research Institute of Sweden for providing me with good experimental data from the Rödhake program.

I am grateful to all my friends, PhD fellows and colleagues for sharing their time, experiences and dreams with me.

Eventually I would like to dedicate this work to my family (Beatriz and Juan D), my parents (Aida and Juan) and my siblings (Heidy and Harvey), for their support.

Abstract

The steadily increasing use of ductile cast iron and the necessity for building larger cast components present new challenges to the designers. In despite of large cast components are designed adhered to standards, unexpected failure sometime occurs. One reason is the inevitable manufacturing defects containing within the cast components that behave like cracks under cyclic loading. In addition the probability of a large defect to be situated at a critical region of the component increases with the size. Another reason is the effect of geometric discontinuities such as holes, threads and fillets, which are part unavoidable of the designs. These discontinuities that are usually called notches disturb the stress field and cause high local stress concentration. Thus dealing with these severe stress risers (defects and notches) is not an easy task. Therefore most designers resort to use very high and unnecessary safety factors.

List of papers

The present thesis is composed by the following four articles:

1. Zambrano HR, Härkegård G. Prediction of the fatigue limit of sharply notched specimens of mild steel. Submitted for publication in Proceedings of the Institution of Mechanical Engineers, Part C, Journal of Mechanical Engineering Science 2011.
2. Zambrano HR, Härkegård G, Stärk KF. Fracture toughness and growth of short and long fatigue cracks in ductile cast iron EN-GJS-400-18-LT. Accepted for publication in Fatigue & Fract Engng Mater Struct 2011.
3. Zambrano HR, Härkegård G. Self-arresting cracks at notches in ductile cast iron. Submitted for publication in Engng Fract Mech 2011.
4. Zambrano HR, Härkegård G. Fatigue testing and modelling of a ring-shaped component of ductile cast iron. To be submitted for publication in Eng Fail Anal 2011.

The article: Zambrano HR, Härkegård G, Self-arresting fatigue cracks at notches in nodular cast iron, Procedia Engineering 2(1)1531-1537, 2010, presented at 10th International Fatigue Congress, Prague, June 2010, was a precursor of paper [3] and has not been included in this thesis.

The article: Zambrano HR, Härkegård G, Stärk K, Short fatigue crack growth in ductile cast iron, presented at the International Symposium on Fatigue Design & Material Defects, Trondheim, May 2011, was a precursor of paper [2] and has not been included in this thesis.

Contents

CHAPTER 1

Introduction

1.1 Objective

The main objective of this work was to study the effect of notches and cracks in the fatigue limit of cast components of ductile cast iron EN-GJS-400-18-LT.

This shall be achieved by:

- Carrying out an initial survey of the different methods to estimate the fatigue limit of notched specimens.
- Establishing the behavior of short cracks in the ductile cast iron EN-GJS-400-18-LT.
- Developing suitable short crack models to predict the fatigue limit of notched components based on self-arrested cracks.
- Using a suitable short crack model to investigate the effect of small defects in components of cast iron, i.e., simulating crack-like defects. Comparing the results with predictions obtained using other fatigue approaches and experimental data.

1.2 Motivation

One of the most common failures of mechanical components is the fatigue failure. This is caused by the initiation and propagation of cracks. These cracks start from regions of very high stress concentration. Moreover this stress concentration is usually caused by structural discontinuities such as holes, notches, shoulders, cracks, defects and scratches. However previous investigations have demonstrated that the effect of the sharp notches on the fatigue limit is not as harmful as indicated by the local stress at the notch root (‘peak-stress’). Therefore, to prevent fatigue failures in components of cast iron, it is very important to investigate the actual effect of sharp notches on this material.

Cast materials such as EN-GJS-400-18-LT and EN-GJS-600-3, frequently contain a variety of defects that are inherent to the cast procedure. Moreover the number and size of defects increase with the size of the components. Consequently the defect distribution (within

the components) ends up controlling the fatigue life. Thus, to estimate the fatigue life of components, it is absolutely necessary to use methods that take into account (directly or indirectly) the effects of small defects in the fatigue life. These small defects are usually considered small cracks; because of the number of the load cycles required to initiate a crack from one of these defects is negligible. However to model successfully the fatigue propagation of these crack-like defects, the short crack behavior has to be considered.

1.3 Short summary of the thesis

This thesis consists of an introduction and four papers, where the effect of sharp notches and cracks on the fatigue limit of components has been addressed.

Initially a compressive investigation about the different methods, available in the literature, to predict the fatigue limit of notched specimens, was carried out in Paper 1. In addition to empirical methods (Peterson, Neuber, stress gradient and theory of the critical distances), fracture mechanics models were also used in Paper 1.

In Paper 2, an extensive test plan was carried out to determine the tensile, fracture and fatigue properties of the ductile cast iron EN-GJS-400-18-LT. In the manuscript, the plain fatigue limit and its mean stress dependence have been discussed. In addition FCG tests were carried out on cracks ranging from a few tenths of a millimeter ('short' cracks) to several millimeters ('long' cracks). Due to previous FCG tests have been limited to positive load ratios, $R > 0$, whereas many cast components are stressed at $R < 0$, thus the FCG tests included measurements at $R = -1$. It is worth pointing out that an original algorithm was implemented to reduce significantly the scatter in the crack growth measurements. Thus crack growths were measured with resolution better than 1 μm. Finally, in Paper 2, the threshold stress intensity range and its load ratio dependence was analyzed.

In Paper 3, the effect of sharp notches in ductile cast iron EN-GJS-400-18-LT has been investigated. Experiments were carried out using double-edge notched specimens with different notch root radii. By judicious selection of the load amplitudes, self-arresting cracks were observed in some of the specimens. In addition two models were developed to analyze the growth of a short crack from the notch root. One model was a generalization of El Haddad's equation to short-crack growth in an inhomogeneous stress field. The other was a slightly modified version of a model by Härkegård based on El Haddad's asymptotic solution for shallow and deep cracks. The predictions were in reasonable agreement with experimental observation.

In Paper 4, the fatigue limit of a ring-shaped specimen of ductile cast iron EN-GJS-600-3 was estimated based on the peak-stress and non-local stress approaches. This analysis was carried out using FEA in combination with the weakest link theory. In addition the influence of small cracks-like defects on the fatigue limit of the ring-shaped specimen was investigated. A short-fatigue-crack-growth model was used to calculate the life of the component. Eventually in this paper the different models were validated experimentally.

CHAPTER **2**

Notch effect

Notches within the components such as holds, fillets, grooves and keyways, cause local stress concentration, because of the abrupt disturbance of the stress field. Due to the high local stress concentration at the notch tip, the fatigue strength of the components is reduced. Such reduction is known as 'the notch effect'.

Different approaches have been proposed to estimate the life of notched components taking the notch effect into account. However a straight-forward approach based on the (normal) 'peak-stress' range $\Delta\sigma = K_t \Delta S$, is still commonly used, where K_t is the elastic stress concentration factor and ΔS the (gross) nominal stress range. Nevertheless experimental evidence shows that sharp notches are less severe in fatigue than indicated by the peak stress cycle at the notch root [5, 6]. Therefore, the peak stress approach leads to very conservative predictions. One reason for this is that the stress field ahead of the notch root decreases very quickly, thus the fatigue crack initiates at the notch root and propagates in a decreasing stress field.

2.1 Empirically based approaches for predicting the notched fatigue limit

Most of text books recommend the use of the classical approaches proposed by Peterson [7] and Neuber [8] to deal with the notch effect [9].

2.1.1 Classical approaches

Peterson suggested considering the stress at a certain point ahead of the notch tip, and Neuber the average of the stress over a certain distance. These two classical approaches were used in Paper 1 to predict the fatigue limit of notched specimens used by Frost [5] to investigate the notch effect in mild steel. Fig. 2.1 shows the fatigue limit predicted by Peterson and Neuber, and experimental data published by Frost [6].

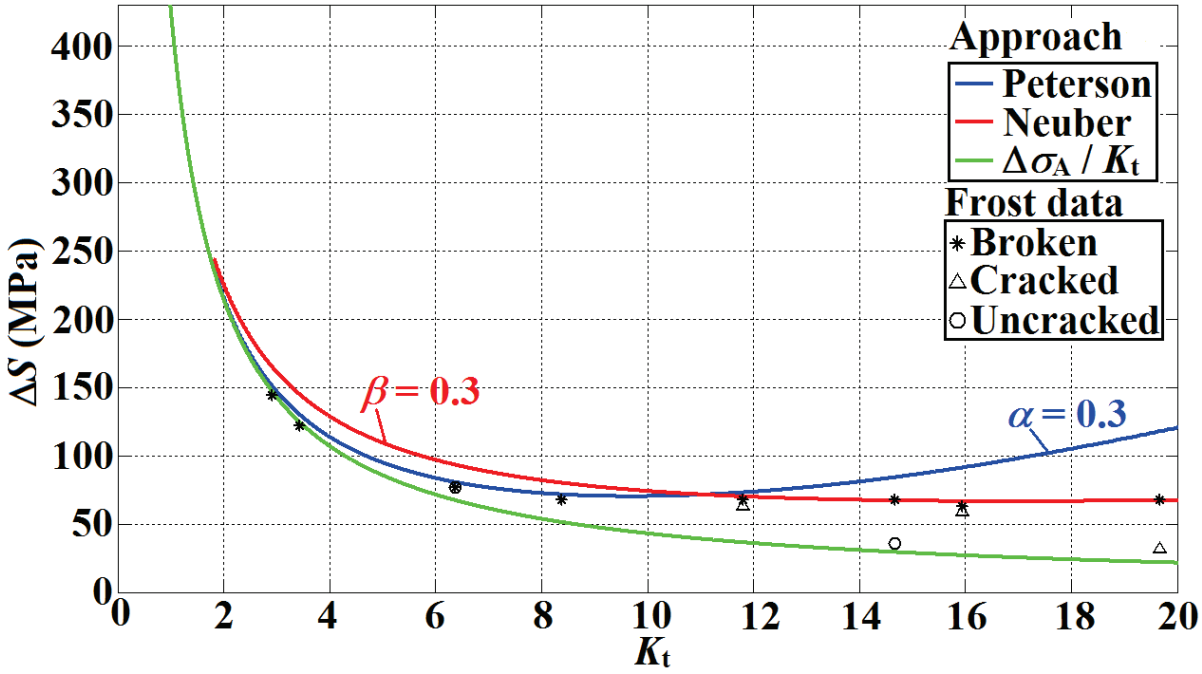

Fig. 2.1: Notched fatigue limit range predicted by Peterson and Neuber.

2.1.2 Stress gradient approach

In addition to the Peterson and Neuber approaches, the stress gradient method proposed by Siebel and Stieler [10] has been used in Paper 1. Siebel and Stieler [10] proposed using the absolute value of the relative stress gradient χ at the notch root

$$\chi = \left| \frac{1}{\sigma} \left(\frac{\mathrm{d}\sigma_y}{\mathrm{d}x} \right)_{x=0} \right|, \tag{2.1}$$

where σ_y is the stress perpendicular to the notch plane ahead of the notch root.

The gradient method for prediction of notched fatigue limit is based on peak stress range $\Delta\sigma = K_t \Delta S_A = s_\chi \Delta\sigma_A$, where s_χ is the notch support factor. An empirical relationship between s_χ and χ proposed by Siebel and Stieler [10] was used in Paper 1 to estimate the notch fatigue limit. Moreover another empirical relationship proposed in the FKM Guideline [11] was also used. Fig 2.2 shows the fatigue limit predicted by these two stress gradient approaches.

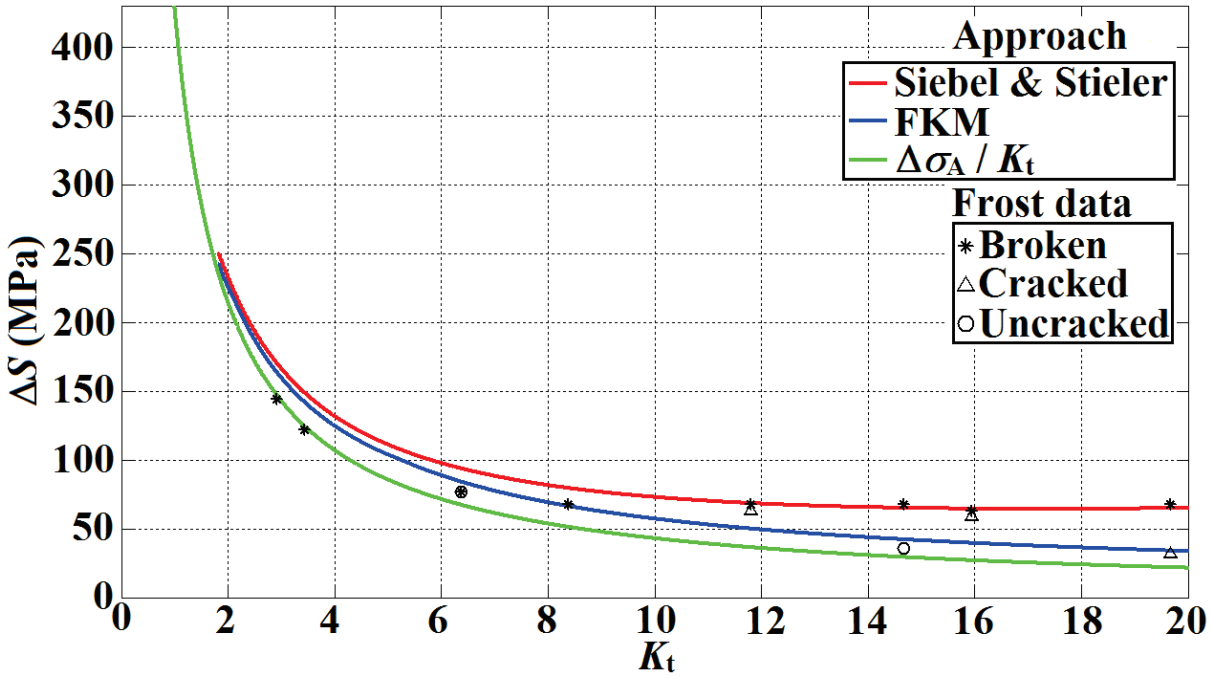

Fig. 2.2: Fatigue limit range predicted by stress gradient approaches for different K_t.

2.1.3 Critical distance approach

The TCD [12] contains four different approaches. In Paper 1, only the point method (PM) has been used. This method predicts the fatigue limit of a component, when the stress range at a distance $L/2$ ahead of the notch root reaches the plain fatigue limit $\Delta\sigma_A$, i.e., $\Delta\sigma_y(y = L/2) = \Delta\sigma_A$. Moreover TCD uses the intrinsic crack depth proposed by EL Haddad et al. [13] as L, viz.,

$$L = \frac{1}{\pi}\left(\frac{\Delta K_{th}}{\Delta\sigma_A}\right)^2 \tag{2.2}$$

Finite element analyses were carried out in Paper 1 to obtain the stress field ahead of the notch tip. Eight different notch radii were modeled in ABAQUS. Fig. 2.3 shows the stress field ahead of the notch root (obtained by means of FEA) for the specimen used by Frost [6]. In addition, Fig. 2.4 shows the fatigue limit as predicted by the point method. The fatigue limit for a crack of depth d = 5.08 mm has also been plotted, using the model proposed by Smith & Miller [14].

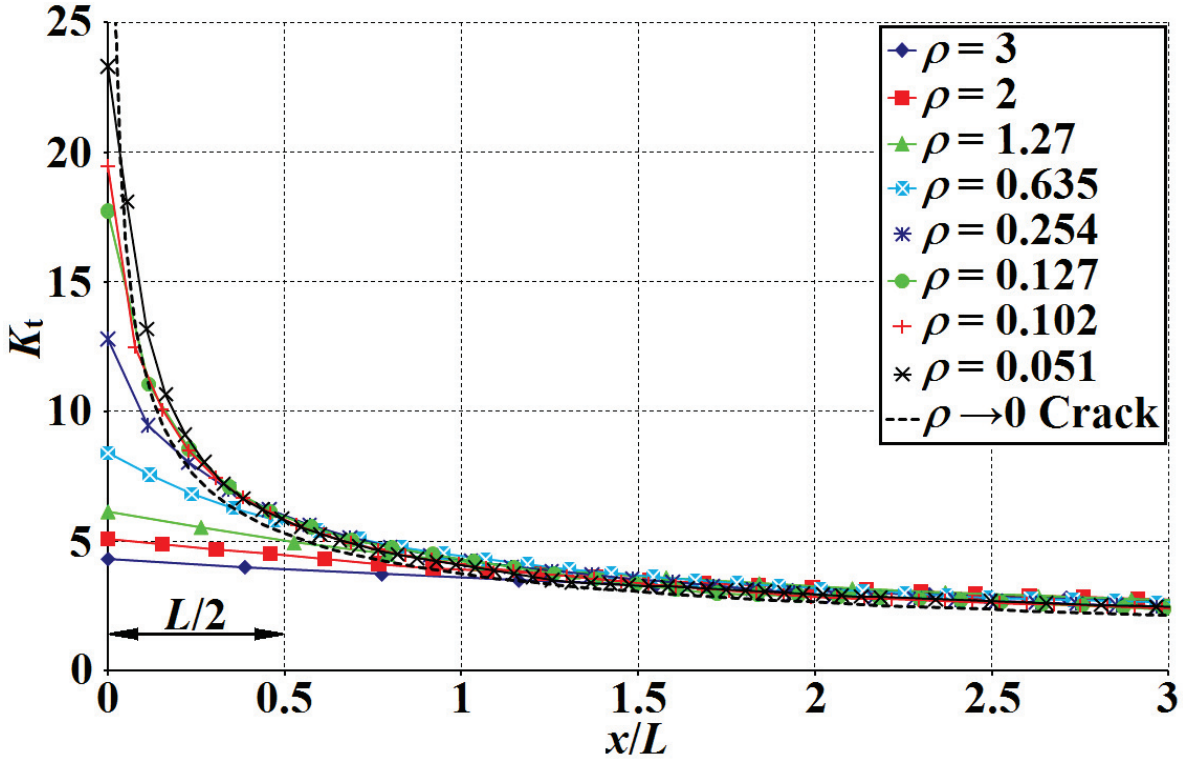

Fig. 2.3: Stress field ahead of the notch root for different notch radii.

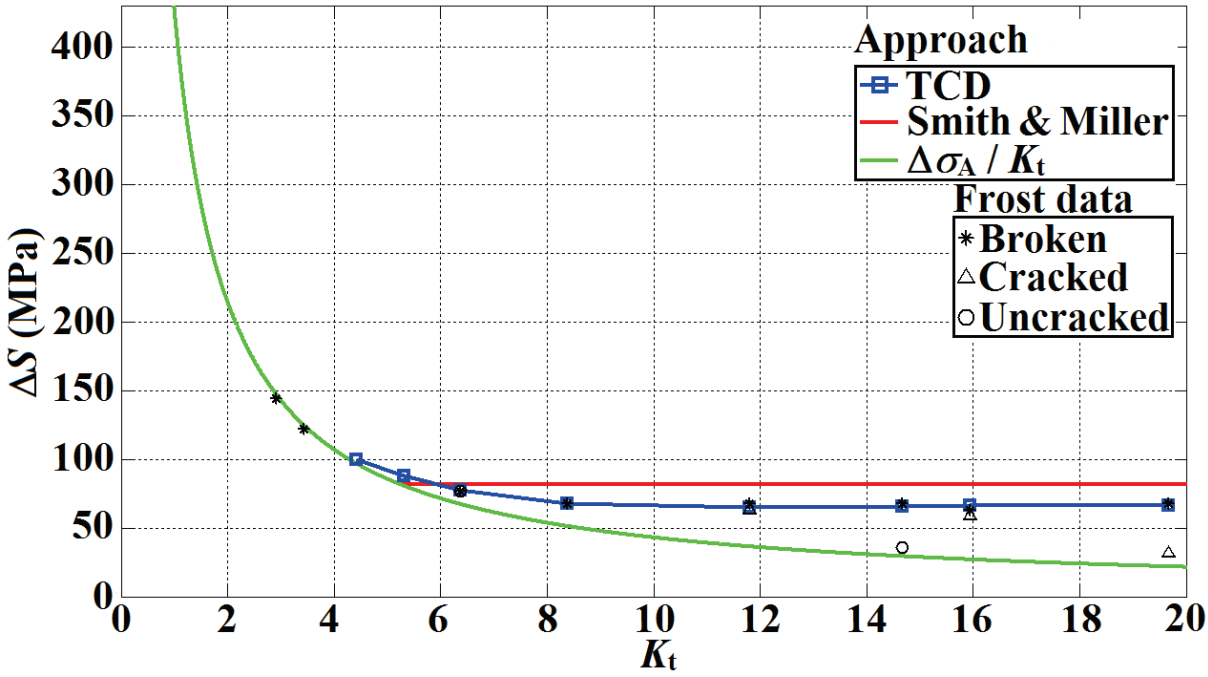

Fig. 2.4: Fatigue limit range predicted by theory of critical distances (PM) for different stress concentration factors.

2.2 Fatigue limit predicted by self-arresting crack modelling

According to Fig. 2.3, the highly stressed region caused by the sharp notch is small, and the stress ahead of the notch root decreases rapidly. Therefore, if the notch is sufficiently sharp, i.e., the stress gradient at the notch root sufficiently high, the crack is arrested and becomes 'non-propagating' after a few tenths of millimetre. Such 'self-arresting' cracks were observed by Frost et al [6] at the notch root of the run-out fatigue specimens.

2.2.1 Short fatigue crack models

Zambrano and Härkegård [3] developed slightly modified versions of models proposed by El Haddad [13] and Härkegård [15]. These models were applied in the present investigation to predict self-arresting cracks in mild steel.

The growth of a short fatigue crack from the notch root has been modeled in Fig. 2.5. The fatigue crack growth models are explained (in details) in [3]. In addition the notched fatigue limit predicted by these models has been presented in Fig. 2.6.

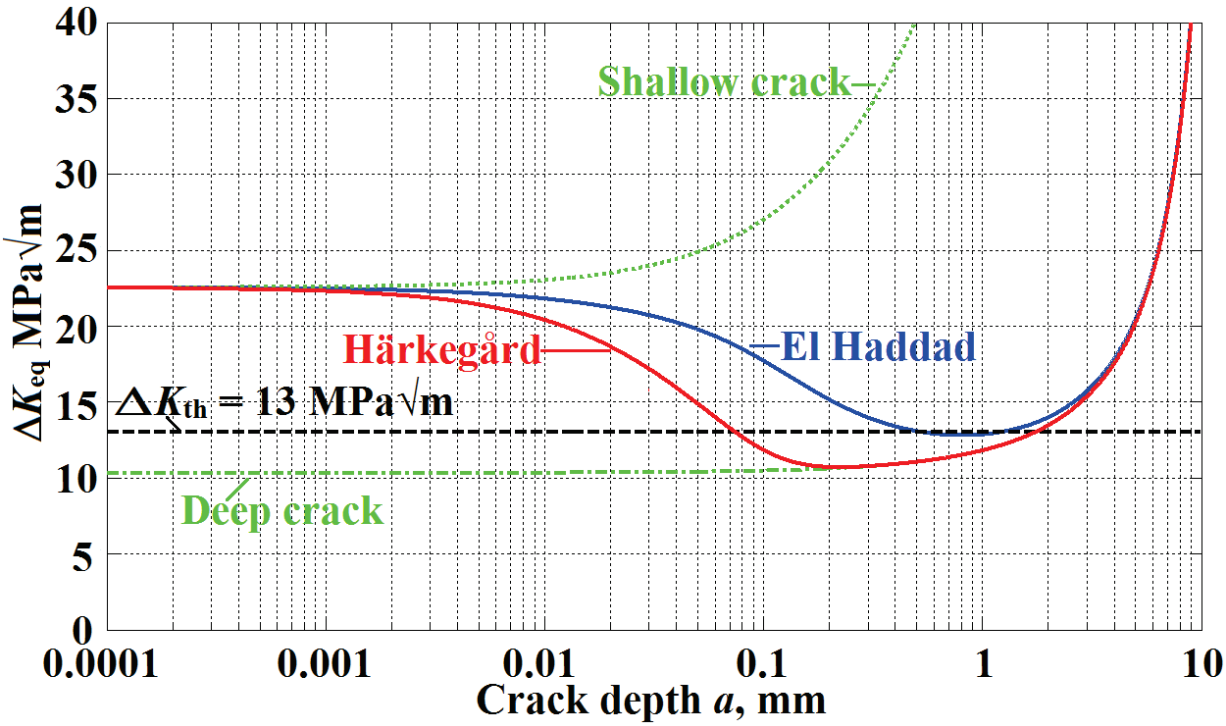

Fig. 2.5: Equivalent stress intensity range vs. crack depth for a specimen with notch root radius $\rho = 0.25$ mm subjected to gross stress rang $\Delta\sigma = 63.2$ MPa.

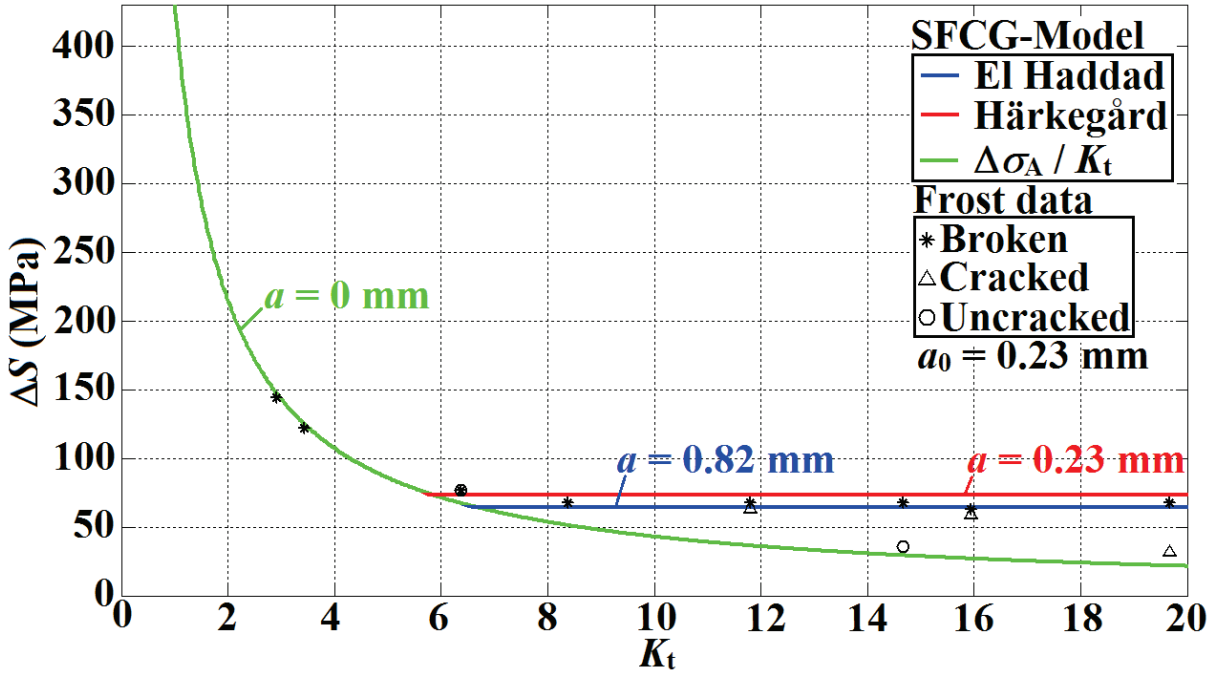

Fig. 2.6: Notched fatigue limit predicted by El Haddad's and Härkegård's models for self-arresting cracks as a function of the stress concentration factor K_t.

CHAPTER **3**

Short and long fatigue cracks in ductile cast iron EN-GJS-400-18-LT

The steady increase in the number and size of wind turbines for the generation of electric power requires improved knowledge of materials data for highly loaded components. Ductile cast iron EN-GJS-400-18-LT [16] is widely used for wind-turbine hub, bearing housing and base-plate. Even in components cast under optimized conditions, the designer must allow for the presence metallurgical defects, e.g., shrinkage cavities, porosity, slag inclusions and degenerate graphite. Under cyclic loading conditions, such defects tend to behave as cracks. Hence, the endurance of cast components is mainly controlled by the growth of fatigue cracks from casting defects [17-22]. To be able to determine the size of permissible defects for a given endurance, the designer needs access to reliable fatigue crack growth (FCG) data. For ductile cast iron EN-GJS-400-18-LT, the availability in the open literature of such data is still very limited [23-25]. Besides, available data typically refer to tests on several-millimeter-long cracks. In many cases, however, fatigue life is dominated by the growth of sub-millimeter cracks [17, 22]. Therefore, in Paper 2, FCG tests have been carried out on cracks ranging from a few tenths of a millimeter ('short' cracks) to several millimeters ('long' cracks). Previous FCG tests have been limited to positive load ratios, $R > 0$, whereas wind turbine load spectra contain a considerable fraction of load cycles with $R < 0$. Thus, the present study includes tests at $R = -1$. In addition the FCG tests were supplemented with fracture toughness measurements at a range of temperatures.

3.1 Microstructure and tensile and fracture toughness properties

The material investigated in Paper 2 was ductile cast iron EN-GJS-400-18-LT. the chemical composition is given in Table 3.1. The microstructure of the material is characterized by spheroidal graphite nodules embedded in a ferritic matrix as shown in Fig. 3.1. The size distribution of the graphite nodules, determined by measuring 790 nodules with diameters ranging between 10 and 120 μm, is shown in Fig. 3.2. The arithmetic mean was found to be $D = 32$ μm, the standard deviation 16 μm.

Table 3.1: Chemical composition (wt. %) of ductile cast iron EN-GJS-400-18-LT, balance Fe.

C	Si	Mn	P	S	Ni	Mg
3.61	2.18	0.23	0.014	0.009	0.088	0.041

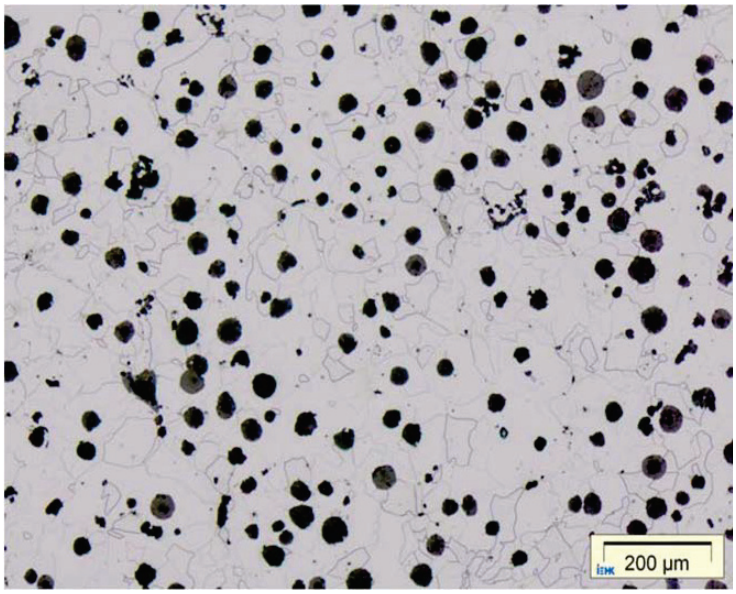

Fig. 3.1: Microstructure of ductile cast iron EN-GJS-400-18-LT.

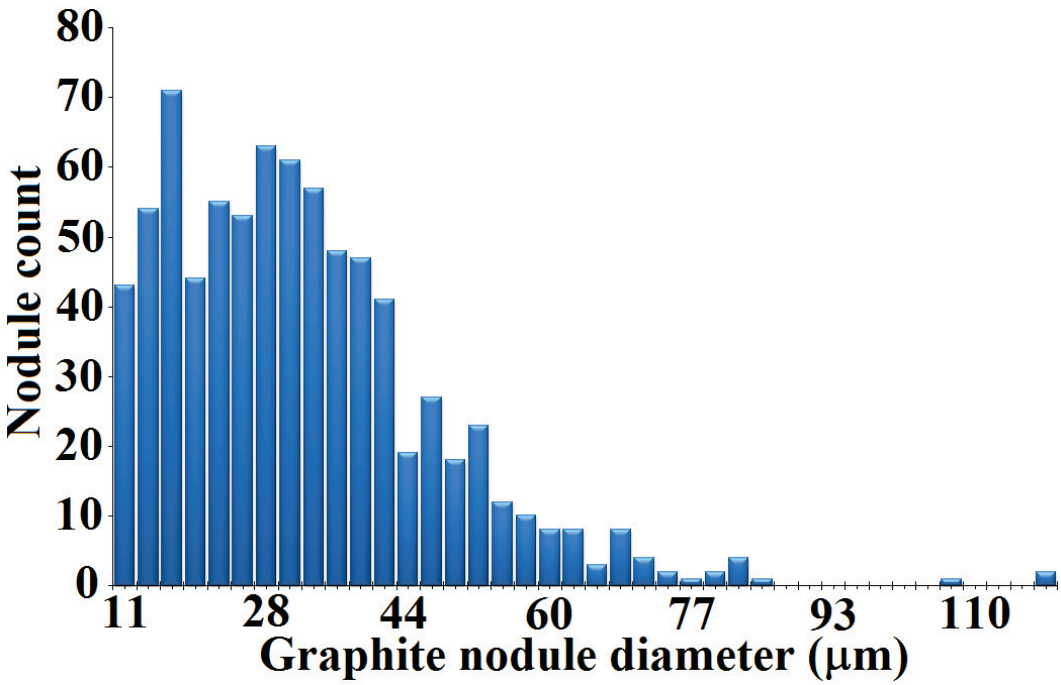

Fig. 3.2: Nodule size distribution for cast iron EN-GJS-400-18-LT.

It is worth pointing out that a cylindrical sample of this material with diameter 21 mm and gage length 100 mm was examined for defects by means of X-ray computed tomography (XCT) [26]. No defects were found above the XCT resolution limit of 0.2 mm. In addition the tensile properties of the cast block satisfy the standard requirements [16].

The fracture toughness was investigated experimentally (in accordance with the ASTM standard [16]) at different temperatures between -38 ^{o}C and 22 ^{o}C. The experimental results are presented in Fig. 3.3. It should be noted that fracture toughness remains nearly constant over the investigated range of temperatures.

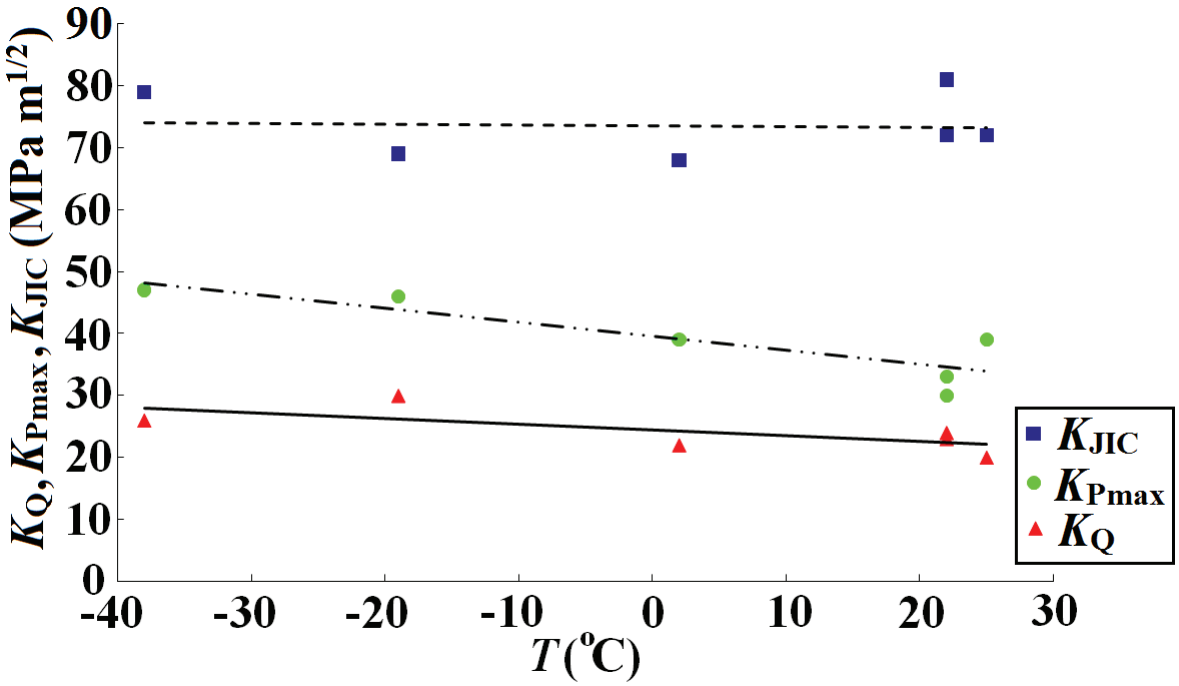

Fig. 3.3: Fracture toughness vs. temperature.

3.2 The plain fatigue limit and its mean stress dependence

In order to determine the fatigue limit of axially loaded plain specimens, a load-increasing procedure due to Denk and Amhof [28] was used. Plain specimens (d = 0) were tested at R = -1 and R = 0. The test specimen and procedure has been explained in details in [2].

The push-pull fatigue limit was in fair agreement with the fatigue limit under rotating bending stated in [16], $\Delta\sigma_W$ = 390 MPa. In addition the following equation has been used to describe the effect of mean stress on the fatigue limit, viz.,

$$\frac{\Delta\sigma}{\Delta\sigma_W}+\left(\frac{\sigma_m}{R_m}\right)^{\delta}=1. \qquad (3.1)$$

A perfect fit to the experimental value is obtained when δ = 1.62. It may be noted that eq. (3.1) reproduces the well-known Gerber parabola [9], when δ = 2 and the (modified) Goodman equation when δ = 1. The Haigh diagram is plotted in Fig. 3.4.

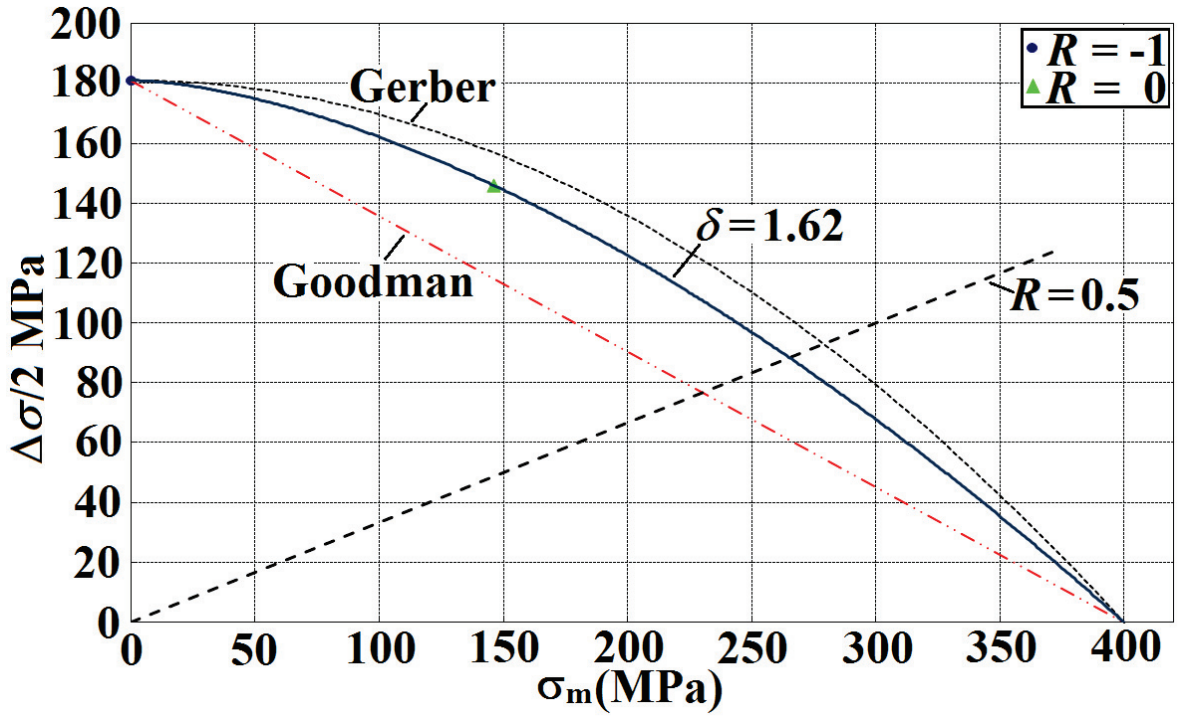

Fig. 3.4: Haigh diagram showing experimental data and (modified) Goodman and Gerber lines.

3.3 Fatigue crack growth testing

FCG tests were carried out on specimens with a starter notch as shown in Fig. 3.4 (ρ = 0.15 mm, d = 0.4 mm and 0.8 mm). Crack growth was monitored by means of the potential drop technique. The starter notches were spark eroded into the specimens. The specimens were subjected to a direct current of 10 amperes, and the potential drop across the fatigue crack was measured with probes located at a distance y = 2 mm from the crack plane; see Figs. 3.4. Moreover an equation given in [29] was used to compute the crack depth. Thus relative potential drop increase, u, was converted into crack depth, a. The scatter was much reduced by suitable averaging of crack depths. Thus, a straight line was fitted to twelve successive calculated crack depths, as presented in Fig. 3.5. The 'representative' (N_j, a_j) was taken at the middle of the line segment. This procedure was repeated by successively moving one data point ahead until all data had been covered. A line segment with a negative slope was neglected.

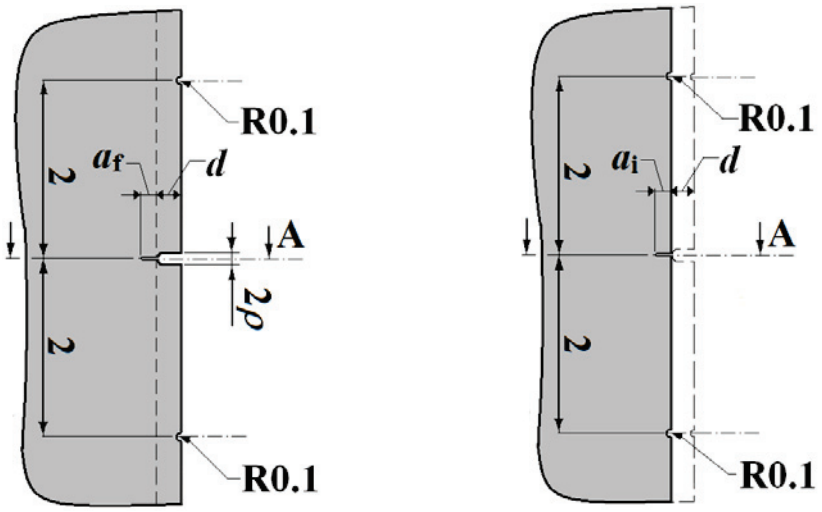

Fig. 3.4: (a) Crack initiated at root of starter notch, end of stage 'i' (b) Cracked specimen after machining away the starter notch, beginning of stage 'p'.

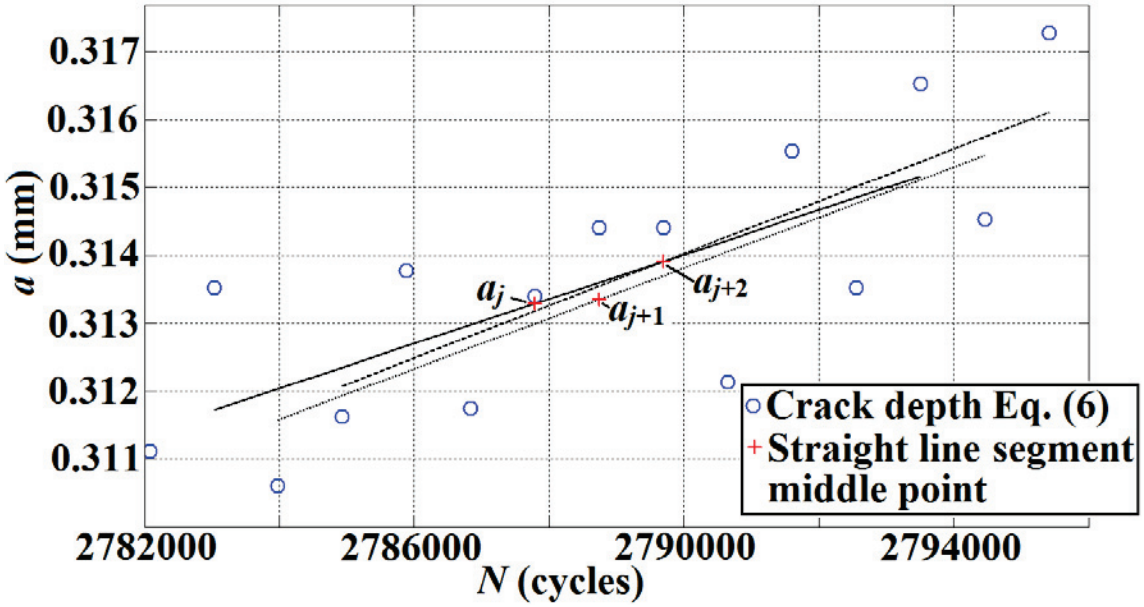

Fig. 3.5: Averaging of crack depths calculated from potential drop measurements.

3.4 Fatigue crack growth of short and long cracks

Fatigue crack growth rates as functions of the stress intensity range for load ratios R = -1, 0 and 0.5 are presented in Figs. 3.6a–c , where the crack depth range associated with a set of test data has also been specified. Whereas long cracks have a well-defined threshold, this is not the case for short cracks.

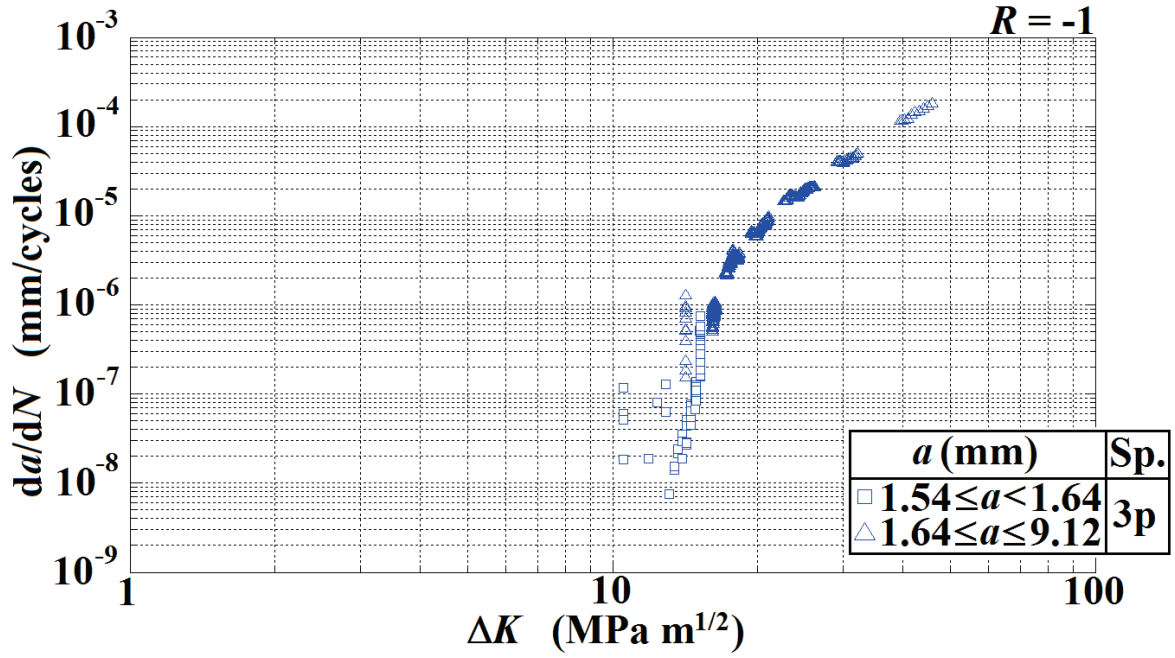
R = -1
da/dN (mm/cycles)
ΔK (MPa m^1/2)
a (mm)
Sp.
1.54≤a<1.64
1.64≤a≤9.12
3p

(a)

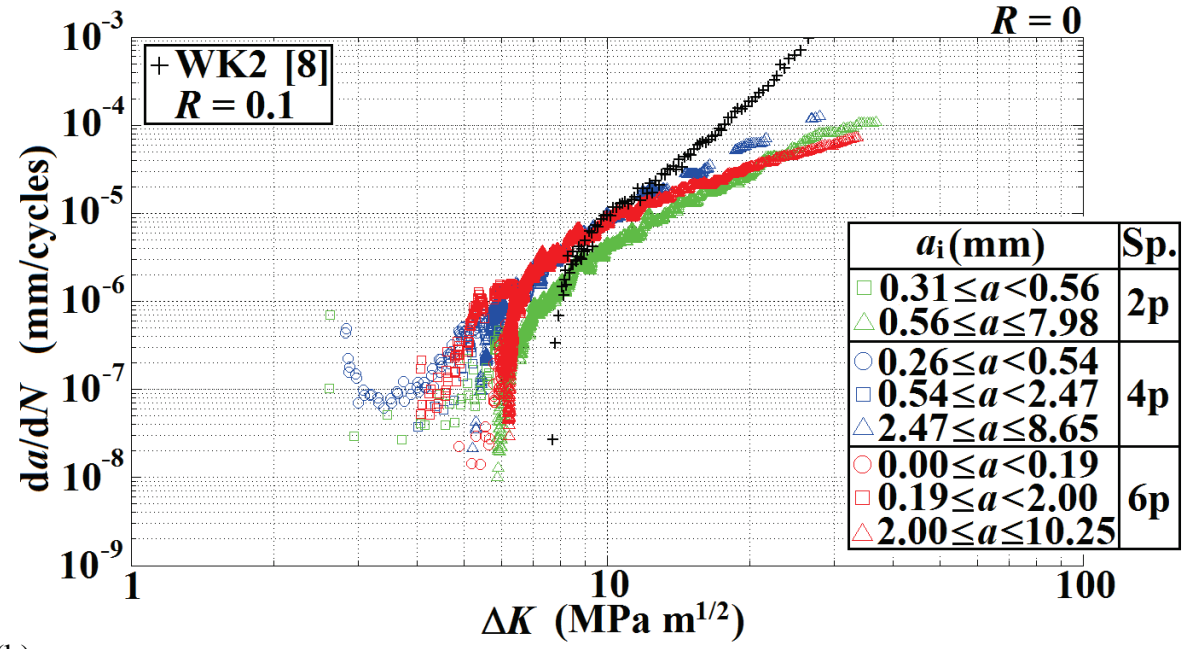
R = 0
+WK2 [8]
R = 0.1
da/dN (mm/cycles)
ΔK (MPa m^1/2)
ai (mm)
Sp.
0.31≤a<0.56
0.56≤a≤7.98
2p
0.26≤a<0.54
0.54≤a<2.47
2.47≤a≤8.65
4p
0.00≤a<0.19
0.19≤a<2.00
2.00≤a≤10.25
6p

(b)

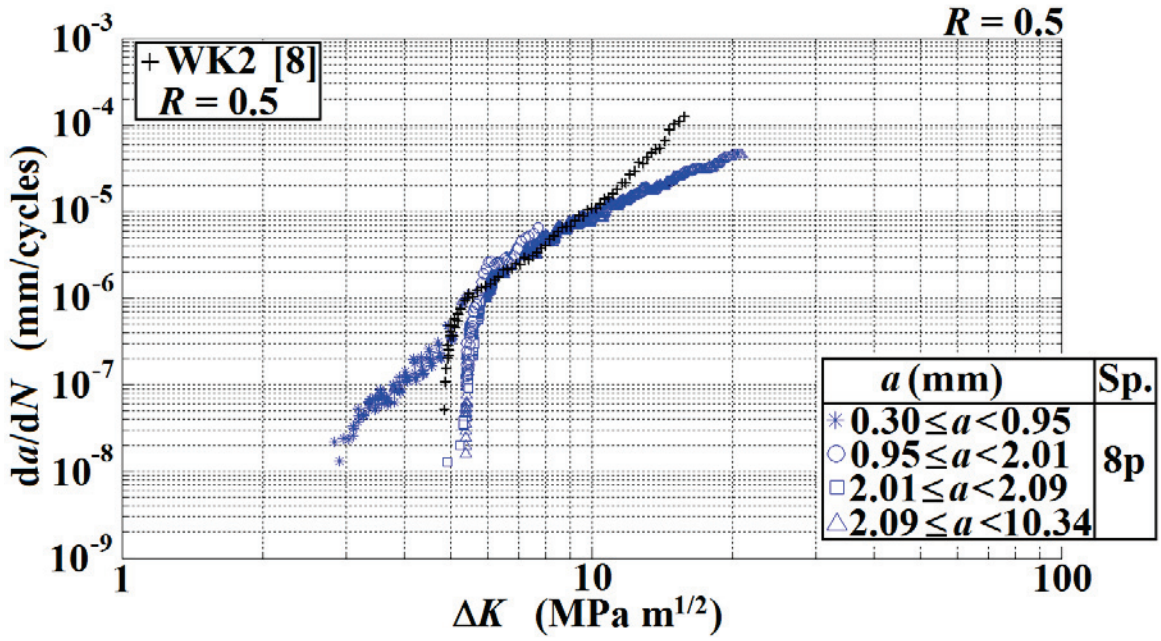

(c)

Fig. 3.6: Fatigue crack growth rate as a function of the stress intensity range at (a) R = -1, (b) R = 0, and (c) R = 0.5.

An equivalent stress intensity range,

$$\Delta K_{\mathrm{eq}} = F\Delta S\sqrt{\pi\left(a + a_0\right)} \tag{3.2}$$

has been used to unify the description of short and long fatigue crack growth [13, 20, 29]. Applying this equation, with the 'intrinsic' crack depth

$$a_0 = \frac{1}{\pi}\left(\frac{\Delta K_{\mathrm{th}}}{1.122\Delta\sigma_{\mathrm{A}}}\right)^2, \tag{3.3}$$

to the present crack growth data yields the results shown in Figs. 3.7 a–c, where da/dN has been plotted against ΔK_{eq}. Moreover long-crack data were used to determine the parameters of the equation proposed by Klesnil and Lukáš [30],

$$\frac{\mathrm{d}a}{\mathrm{d}N} = C\left(\Delta K_{\mathrm{eq}}^{m} - \Delta K_{\mathrm{th}}^{m}\right) \tag{3.4}$$

by means of a least-squares fit. Moreover Table 3.2 summarizes the fatigue properties of ductile cast iron EN-GJS-400-18-LT.

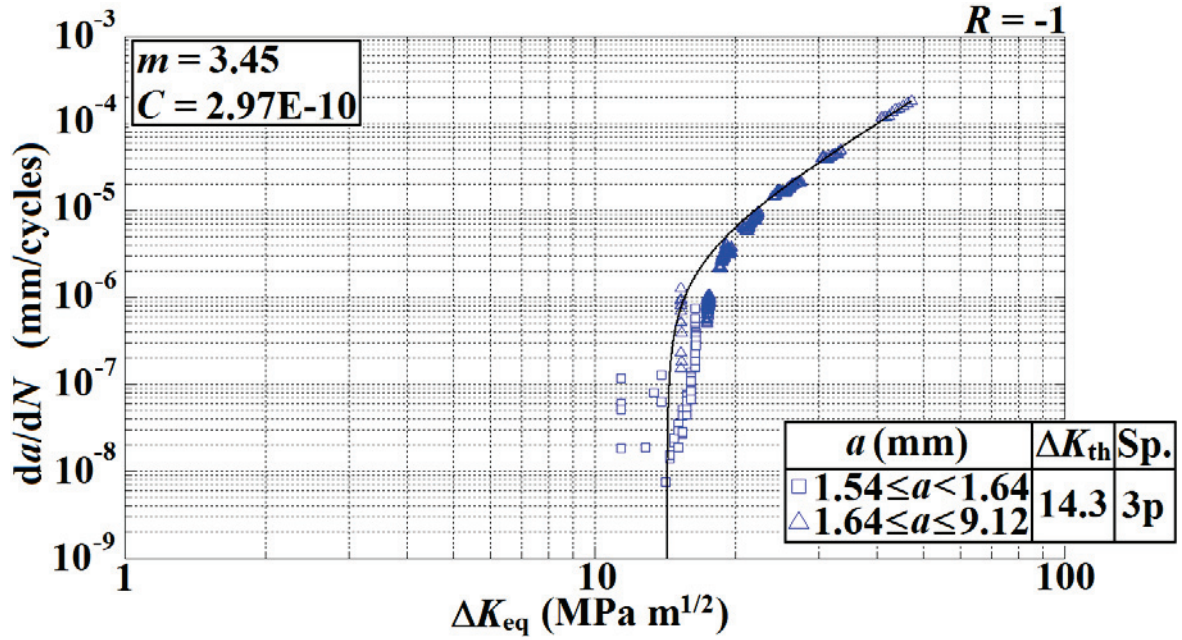
R = -1
m = 3.45
C = 2.97E-10
da/dN (mm/cycles)
ΔKeq (MPa m1/2)
a (mm)
ΔKth
Sp.
1.54≤a<1.64
1.64≤a≤9.12
14.3
3p

(a)

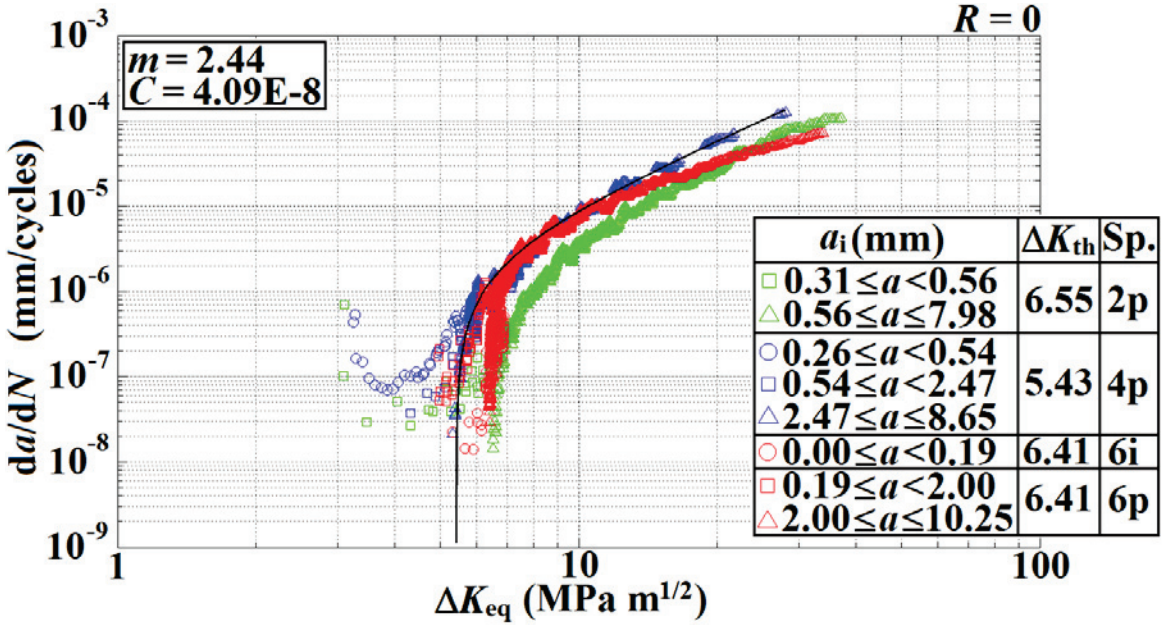
R = 0
m = 2.44
C = 4.09E-8
da/dN (mm/cycles)
ΔKeq (MPa m1/2)
ai (mm)
ΔKth
Sp.
0.31≤a<0.56
0.56≤a≤7.98
6.55
2p
0.26≤a<0.54
0.54≤a<2.47
2.47≤a≤8.65
5.43
4p
0.00≤a<0.19
6.41
6i
0.19≤a<2.00
2.00≤a≤10.25
6.41
6p

(b)

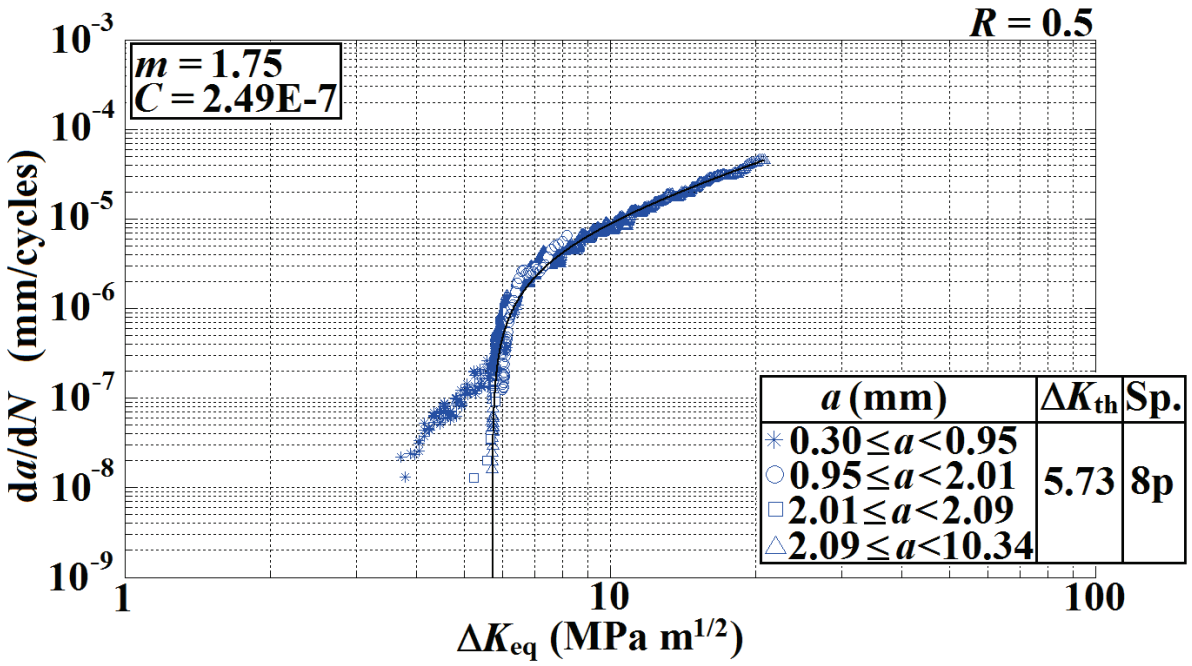

(c)

Fig. 3.7: Fatigue crack growth rate as a function of the equivalent stress intensity range at (a) R = -1, (b) R = 0, and (c) R = 0.5.

Table 3.2: Fatigue properties of ductile cast iron EN-GJS-400-18-LT.

Specimen #	R	$\Delta\sigma_A$ [a] (MPa)	ΔK_{th} (MPa√m)	a_0 (mm)	C [c]	m	max ΔK [d] (MPa√m)
3p	-1	362	14.3	0.396	$2.97\cdot10^{-10}$	3.45	50
2p	0	292	6.55	0.127	-	-	-
4p	0	292	5.43	0.087	$4.09\cdot10^{-8}$	2.44	30
6p	0	292	6.41	0.122	-	-	-
-	0	292	6.13[b]	-	-	-	-
8p	0.5	177	5.73	0.266	$2.49\cdot10^{-7}$	1.75	20

[a] Due to Fig. 8.
[b] Mean value of specimens 2p, 4p and 6p.
[c] Units in eq. (11) are mm/cycle and MPa√m.
[d] Upper limit for C and m to be valid.

3.5 The threshold stress intensity range and its load ratio dependence

The measured ΔK_{th} data can be fitted using an equation proposed by Mann [31], viz.,

$$\Delta K_{th} = \Delta K_{eff,th}\left(1-R\right)/\left(1-R_{eff}\right), \tag{3.5}$$

where $\Delta K_{eff,th}$ signifies the closure free threshold stress intensity range. Tentatively, $\Delta K_{eff,\,th}$ has been set equal to the threshold stress intensity range, ΔK_{th}, at the highest applied load ratio, $R = 0.5$. $R_{eff} = 0.18$ is a least-squares fitting parameter representing the minimum load ratio, at which crack growth is closure free. More fatigue experiments are recommended for $R > 0.5$ to establish whether ΔK_{th} remains constant beyond $R = 0.5$. Hübner et al. [23] reported ΔK_{th} = 7.8, 6.5 and 4.9 MPa√m for WK2 at R = 0.1, 0.3 and 0.5, respectively. Fitting these data to eq. (3.5), and (again) assuming $\Delta K_{eff,\,th} = \Delta K_{th}(R = 0.5)$, yields $R_{eff} = 0.45$. ΔK_{th} vs. R for the two investigations is shown in Fig. 3.8.

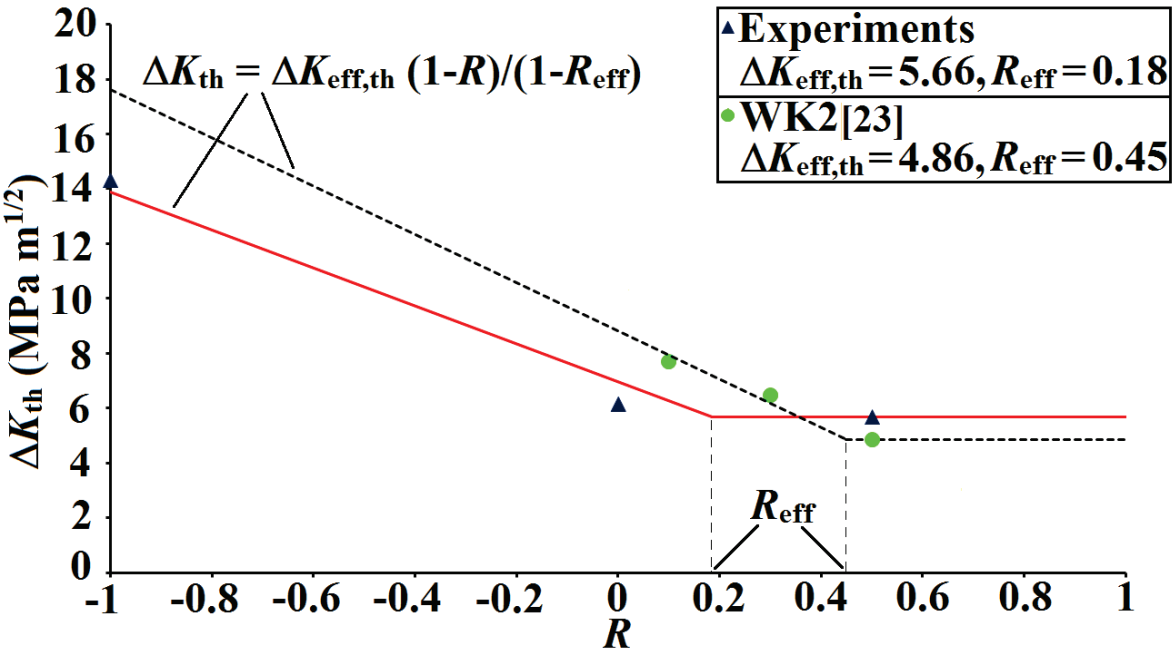

Fig. 3.8: R-ratio effect on ΔK_{th} for ductile cast iron EN-GJS-400-18-LT

CHAPTER **4**

Experimental investigation and modelling of Self-arresting cracks at notches in ductile cast iron

A straight-forward prediction of the expected life of a mechanical component is based on the (normal) peak stress range, $\Delta\sigma = K_t \Delta S$, where K_t is the elastic stress concentration factor and ΔS the nominal stress range. It is well known that notches are less severe in fatigue than indicated by the peak stress [9, 15]. One reason for this is the limited size of the highly stressed region, which implies a small probability of finding a 'weak spot' there. Another reason is the fact that the fatigue crack propagates in a decreasing stress field, which means that the crack 'driving force' is less than in a plain specimen. If the notch is sufficiently sharp, i.e., the stress gradient at the notch root sufficiently high, the crack may be arrested and become 'non-propagating' after a few tenths of millimetre. Such 'self-arresting' cracks have been observed and modelled in several investigations [5, 6, 14, 32-34].

In Paper 3, a study of the notched fatigue limit, ΔS_A, of cast iron EN-GJS-400-18-LT has been performed. Slightly modified versions of models proposed by El Haddad [7] and Härkegård [8] have been applied to a crack growing at the root of a notch in a plane and an axisymmetric specimen. Thus, it has been possible to predict the occurrence of self-arresting cracks. In addition the models were verified experimentally.

4.1 Material and experimental method

4.1.1 Material and test specimens

The material used in the experiments described in Paper 3 was the same ductile cast iron investigated in [2], which has been described in details in Chapter 3. A total of nine rectangular notched specimens were machined. The different notch root radii, ρ, and their respective stress concentration factors, K_t, have been specified In Table 4.1.

Table 4.1: Notch parameters, gross nominal stress range, and dimensions of self-arrested cracks.

Specimen #	ρ (mm)	K_t	ΔS (MPa)	a (mm)	$2c$ (mm)
A1	0.19	12.6	56.7	0.70	Through
A2	0.19	12.6	77.3	Fracture	Fracture
B1	0.46	8.40	67.0	0.65	5.34
B2	0.46	8.40	77.3	Fracture	Fracture
C1	0.59	7.56	72.1	0.67	5.77
C2	0.59	7.56	82.5	Fracture	Fracture
D1	0.77	6.72	67.0	-	Crack
D2	0.77	6.72	77.3	1.10	5.2
E1	1.5	6.72	82.4	No crack	No crack

4.1.2 Fatigue tests

The notched specimens were tested under fully reversed axial loading (R = -1). A travelling microscope was used to inspect the notch root for cracks as shown in Fig. 4.1a. Self-arresting cracks found in specimens C1, D2 and B1 has been shown in Fig. 4.1c-d. Table 4.1 summarizes the applied gross nominal stress ranges, ΔS, and the dimensions of the self-arrested cracks found at the notch root after $2 \cdot 10^6$ cycles.

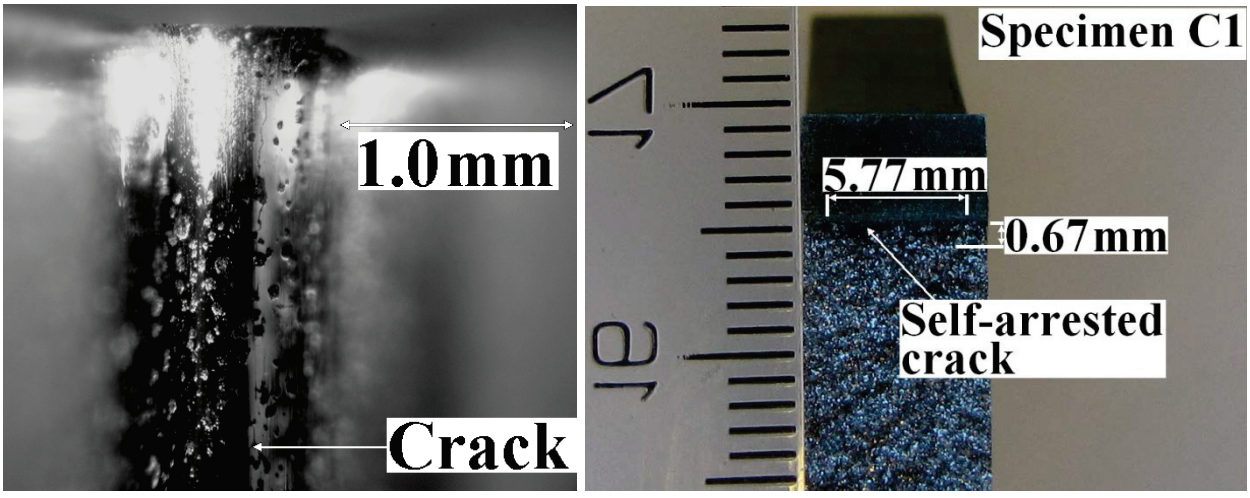

(a) (b)

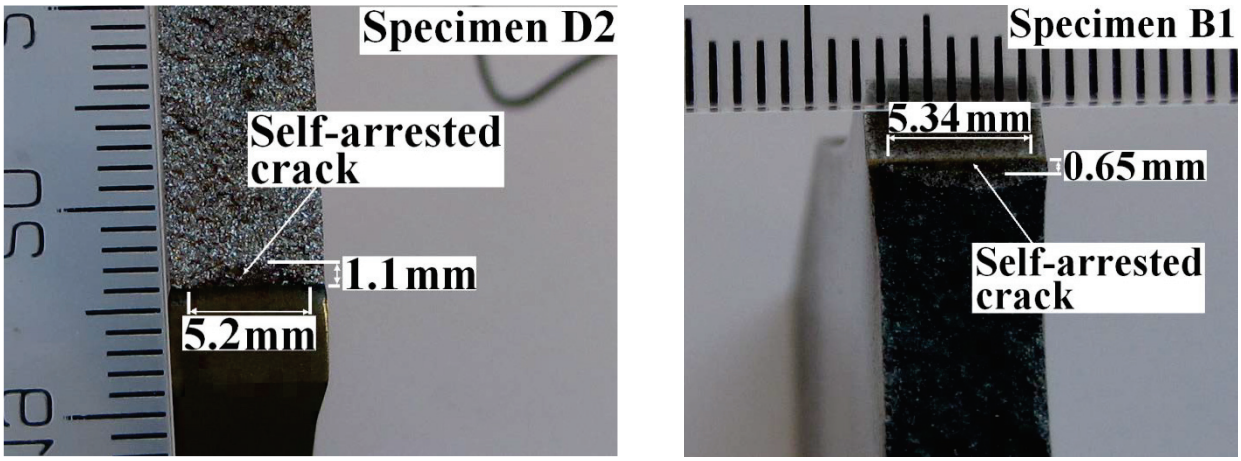

(c) (d)

Fig. 4.1: Crack localized at the notch root (a) just before breaking specimen B1 open and after breaking specimens (b) C1, (c) D2 and (d) B1 open.

4.2 Modelling of self-arresting cracks

4.2.1 Stress intensity range of a crack at the root of a notch

Assuming that the stress intensity range for an arbitrary crack depth may be written as

$$\Delta K = F\left(\frac{a+\theta d}{w}\right)\Delta S\sqrt{\pi\left(a+\theta d\right)},\quad 0\le\theta<1, \tag{4.1}$$

where the crack geometry factor, F, is that of a surface through-crack (or circumferential crack) of depth $a + d$. In addition the transition (or interpolation) function θ is given by:

$$\theta = 1-\mathrm{e}^{-a/a}, \tag{4.2}$$

where the crack depth characterising the transition between shallow and deep cracks is given by

$$a^{*} = d\Big/\left(K_{\mathrm{t}}^{2}-1\right). \tag{4.3}$$

Eq. (4.1), with θ from eq. (4.2), has been plotted in Fig. 4.2 together with the shallow and the deep crack asymptotes. A similar equation for ΔK by Liu and Mahadevan [35] approaches the deep crack asymptote more reluctantly.

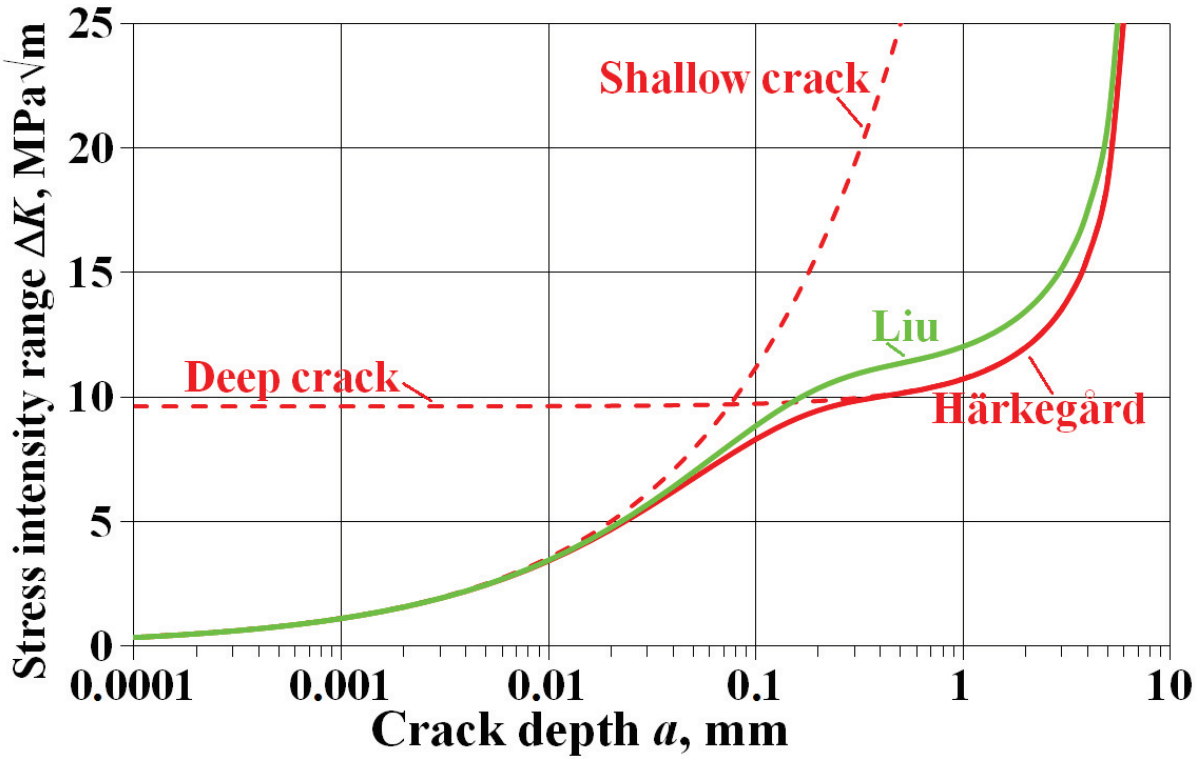

Fig. 4.2: Approximate stress intensity range and shallow and deep crack asymptotes for the double-edge notched plate with $\Delta S = 67$ MPa.

4.2.2 Equivalent stress intensity range based on El Haddad's correction for a short crack in a homogeneous stress field

Using the model by El Haddad et al. [13] to describe the stress intensity range required to propagate a (short) surface crack yields the short-crack corrected 'equivalent' stress intensity range

$$\Delta K_{eq} = 1.122\Delta S\sqrt{\pi\left(a+a_0\right)} = 1.122\Delta S\sqrt{\pi a}\sqrt{1+a_0/a} = \Delta K\sqrt{1+a_0/a}, \qquad (4.4)$$

where the 'intrinsic' crack depth, a_0, is given by eq. (3.3).

If it is tacitly assumed that eq. (4.4) can be generalised to an arbitrary cracked body, as suggested in [34] and [36], eq. (4.1) for a notched member immediately yields

$$\Delta K_{\mathrm{eq}} = F\left(\frac{a+\theta d}{w}\right)\Delta S\sqrt{\pi\left(a+\theta d\right)}\sqrt{1+a_0/a}, \qquad (4.5)$$

4.2.3 Equivalent stress intensity range from an adaptation by Härkegård of El Haddad's short-crack model to a crack growing from a notch in a finite body

Härkegård [32] noted that both the shallow and the deep crack asymptotes for the stress intensity range of a notched member could be consistently corrected for short cracks

using the model by El Haddad et al. [13]. Thus, the asymptotic equivalent stress intensity range for a shallow crack ($a << a^*$) at the notch root becomes

$$\Delta K_{eq} = 1.122 K_t \Delta S \sqrt{\pi (a + a_0)} = 1.122 \Delta S \sqrt{\pi \left(K_t^2 a + K_t^2 a_0 \right)}, \tag{4.6}$$

and for a deep crack ($a >> a^*$)

$$\Delta K_{eq} = F\left(\frac{a+d}{w} \right) \Delta S \sqrt{\pi (a + d + a_0)}. \tag{4.7}$$

Thus an equivalent stress intensity range for an arbitrary crack depth may be written as

$$\Delta K_{eq} = F\left(\frac{a+\theta d}{w} \right) \Delta S \sqrt{\pi \left(a + \theta d + \theta a_0 + (1+\theta) K_t^2 a_0 \right)}. \tag{4.8}$$

4.2.4 Self-arresting cracks in double-edge notch specimens

Fig. 4.3 shows ΔK_{eq} according to eqs. (4.5), 'El Haddad', and eq. (4.8), 'Härkegård', as functions of the crack depth a for specimen B1.

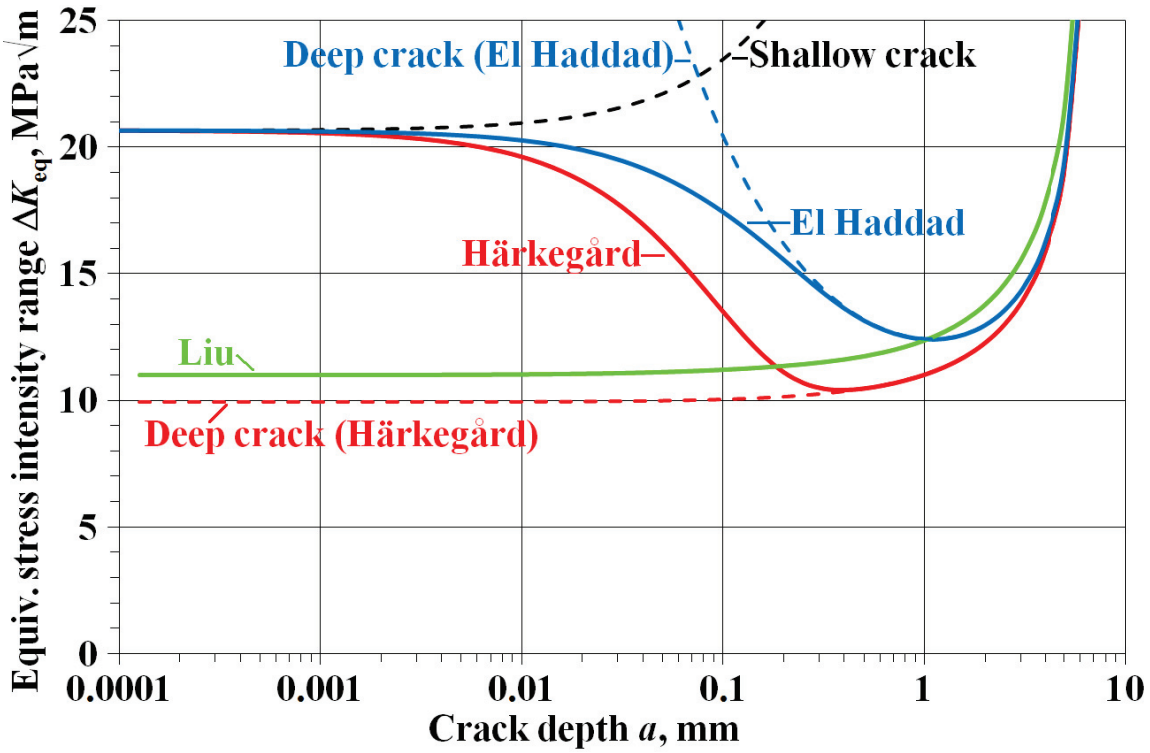

Fig. 4.3: Equivalent stress intensity range for double-edge notched specimen B1 subjected to the gross stress range $\Delta S = 67$ MPa.

Fig. 4.4 shows all three predictions plotted in a 'Frost' diagram. In the present case, there is good agreement between experimental observations (fracture requires $\Delta S > 77$–82 MPa, and arrested cracks have depths in the range $a = 0.65$–1.1 mm) and the El Haddad predictions (fracture requires $\Delta S > 77$ MPa, arrested crack depth $a < 1$ mm), whereas Liu and Mahadevan, Härkegård, and Smith and Miller yield non-conservative predictions.

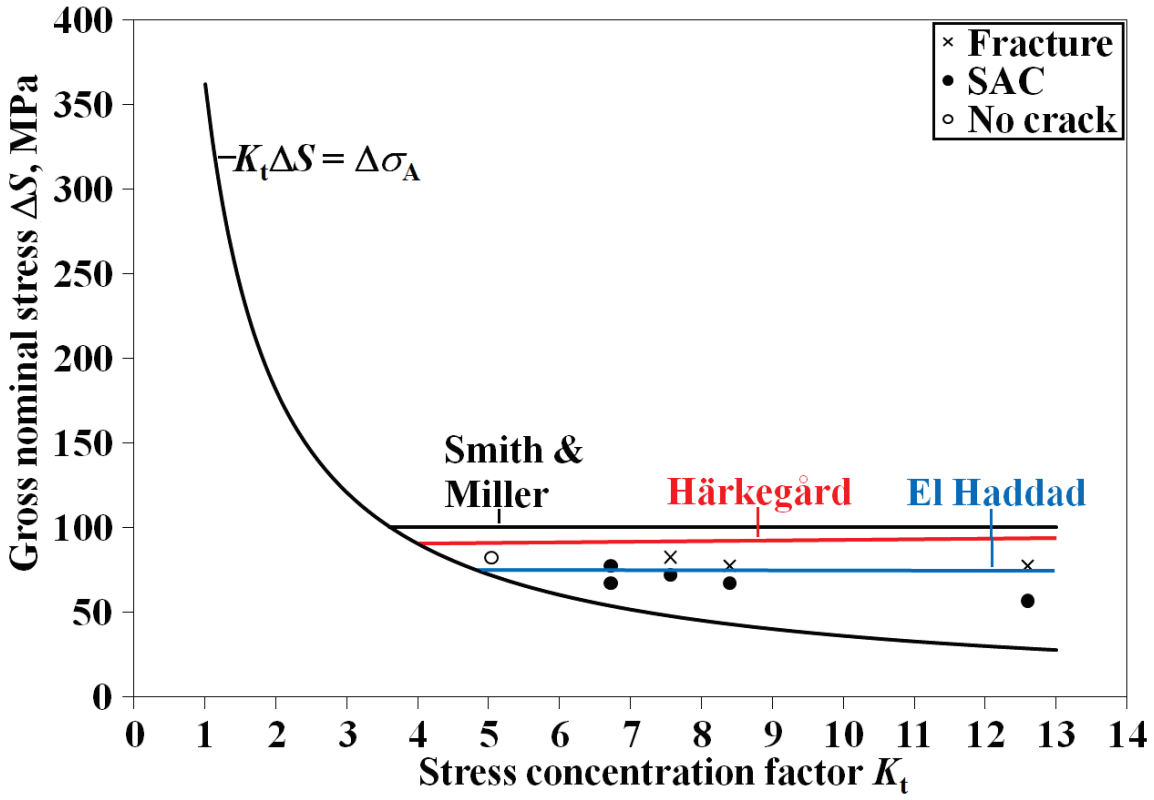

Fig. 4.4: Frost diagram for double-edge notched specimens of cast iron EN-GJS-400-18-LT. Comparison between experimental observations and predictions due to Smith and Miller [14], El Haddad [13], eq. (4.5), and Härkegård [32], eq. (4.8).

4.2.5 Self-arresting cracks in circumferentially notched rotating bending specimens

In Paper 3, the self-arrest of a crack at the root of a sharp notch in an axisymmetric specimen subjected to rotating bending was analysed. The material considered was ductile cast iron with similar properties as EN-GJS-400-18-LT. The fatigue investigation was reported by the British Cast Iron Research Association, BCIRA. The results were in excellent agreement with the predictions by 'Härkegård', whereas the 'Smith and Miller' prediction is on the non-conservative side. The 'El Haddad' prediction, finally, is distinctly conservative. A likely reason for this is the slow convergence of eq. (4.5) to the deep crack asymptote according.

4.2.6 Prediction of the threshold stress intensity range for ductile cast iron based on the plain and notched fatigue limits

The threshold stress intensity range was estimated based on the data listed in the European Standard [16] in Table 4.2. From this table can be concluded that the notched fatigue limit is nearly proportional to the plain fatigue limit, which would, unexpectedly, indicate the 'notch sensitivity' to be nearly independent of the tensile strength of the material. For most engineering alloys, the notch sensitivity is observed to increase with the strength of the material [9].

Table 4.2: Plain and notched (Fig. 9) fatigue limits of ductile cast irons and the associated threshold stress intensity ranges based on self-arrested crack analyses.

Ductile cast iron	$\Delta\sigma_A$ (MPa)	ΔS_A (MPa)	ΔK_{th} (MPa$\sqrt{m}$)
EN-GJS 350-22	360	48.2	13
EN-GJS 400-18	390	51.6	14
EN-GJS 450-10	420	54.1	14.5
EN-GJS 500-7	448	56.7	15.2
EN-GJS 600-3	496	63.0	16.8
EN-GJS 700-2	560	71.0	19
EN-GJS 800-2	608	77.0	20.6
EN-GJS 900-2	634	80.3	21.5

CHAPTER **5**

Fatigue testing and modelling of a ring-shaped component of ductile cast iron.

Despite of rigorous quality control during the casting process, small microstructural irregularities remain within the components. Thus, small flaws such as micro-shrinkages, gas pores and inclusions act as sites for fatigue crack initiation [18, 19, 38]. The size and distribution of such defects are random variables. However, the majority of methods for assessing fatigue life are deterministic, i.e., material properties including defect size are considered as predetermined quantities, neglecting the random nature of these parameters. The most common fatigue approach is the peak-stress method. This method does not take into account the statistical or geometrical size effect [9]. The former is related to the probability of initiating a fatigue crack at a (random) defect [39], the latter to the growth of a fatigue crack in a diminishing stress field [20]

In Paper 4, the fatigue limit of a diametrally loaded ring-shaped specimen made of ductile cast iron will be estimated based on different approaches. Finite element analysis will be used, in combination with the weakest link theory, to carry out a non-local fatigue assessment. The influence of small defects on the fatigue limit of the specimen will also be considered. The predictions of the different models will be compared with experimental observations.

5.1 Material properties and component testing

5.1.1 Material

The material used in Paper 4 was ductile cast iron EN-GJS-600-3 [7]. The microstructure of this material is characterized by spheroidal graphite nodules embedded in a pearlitic-ferritic matrix. The mechanical properties were obtained from the European Standard [16].

5.1.2 Ring-shaped component

Geometry and dimensions of the ring-shaped specimen are given in Fig. 5.1. Thirty-seven specimens were cast. The inside of the specimen was machined, and the rest of the surface was left in the as-cast condition.

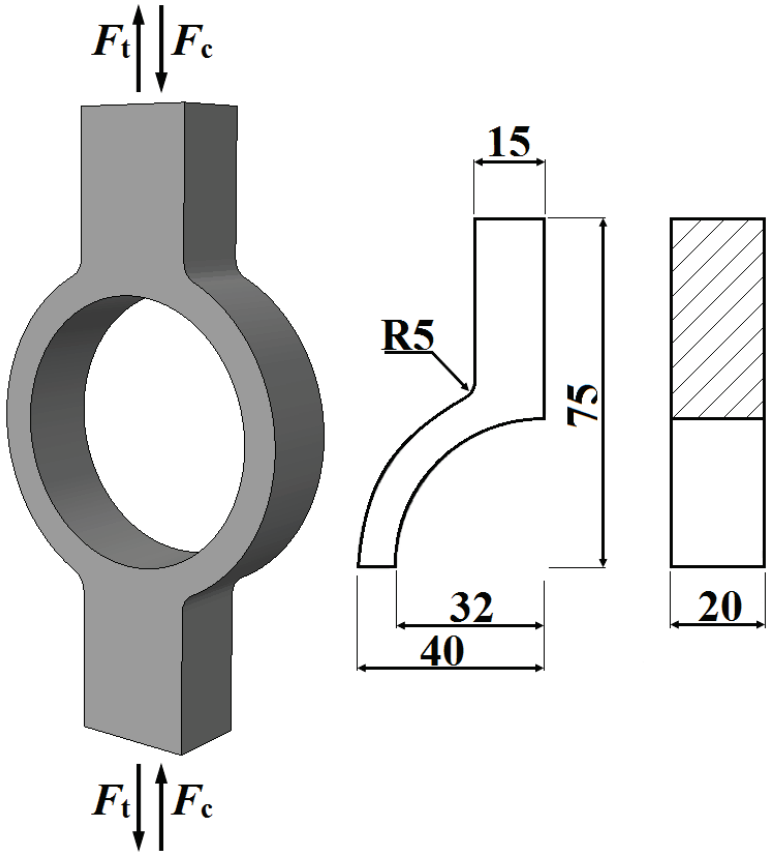

Fig. 5.1: Ring-shaped specimen geometry.

5.1.3 Experimental results

The force amplitude, F_a, has been plotted against the number of cycles for failures and runouts in Figs. 5.2a and b. The probability of failure for a given force amplitude has been estimated by means of $P_f = n_f /(n_t+1)$, where n_f is the number of failed specimens and n_t the total number of specimens tested at this force amplitude. Assuming the probability of failure to be described by a two-parameter Weibull distribution [8],

$$P_f = 1 - 2^{-(F_a/F_A)^b}, \tag{5.1}$$

maximum likelihood was used to estimate the parameters F_A (median fatigue limit) and b (Weibull exponent or shape parameter) to the experimental results.

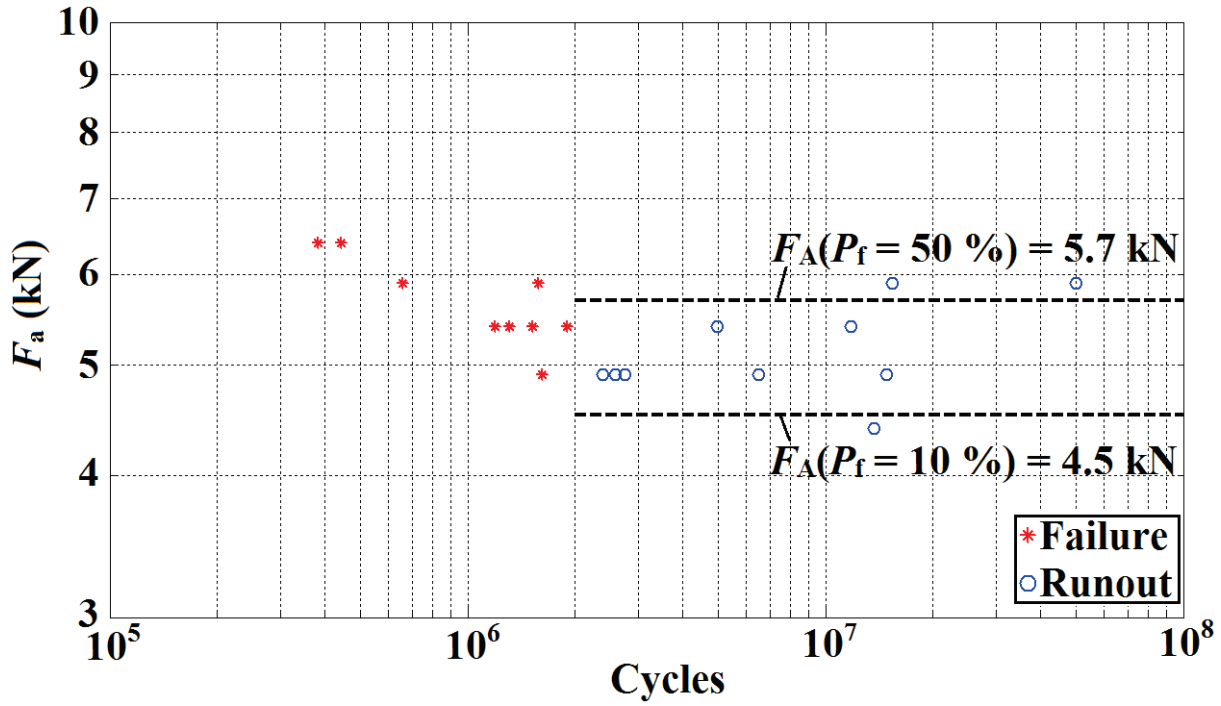

(a)

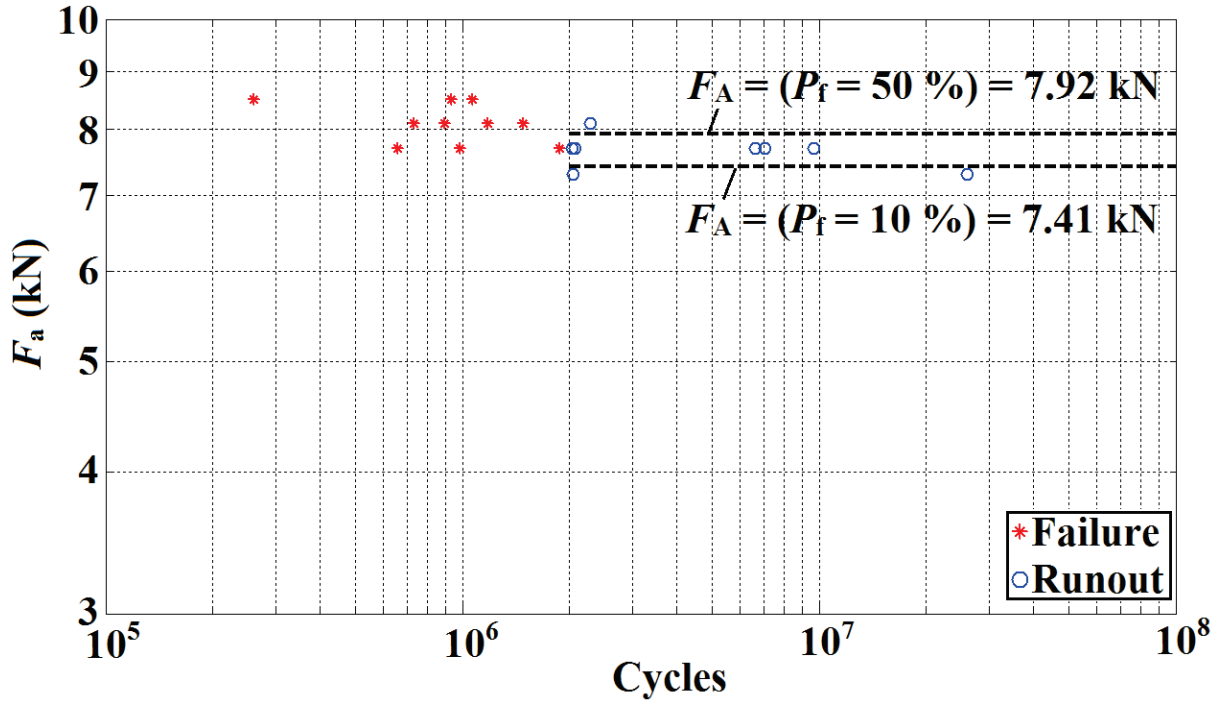

(b)

Fig. 5.2: Force amplitude vs. number of cycles and fatigue limit at P_f = 50 % and P_f = 10 % for (a) tensile and (b) compressive testing.

5.2. Finite element analysis of the ring-shape specimen

A quarter of the ring was modelled in ABAQUS using second-order, 20-node hexagonal elements with reduced integration (C3D20R). The results are shown in Fig. 5.3.

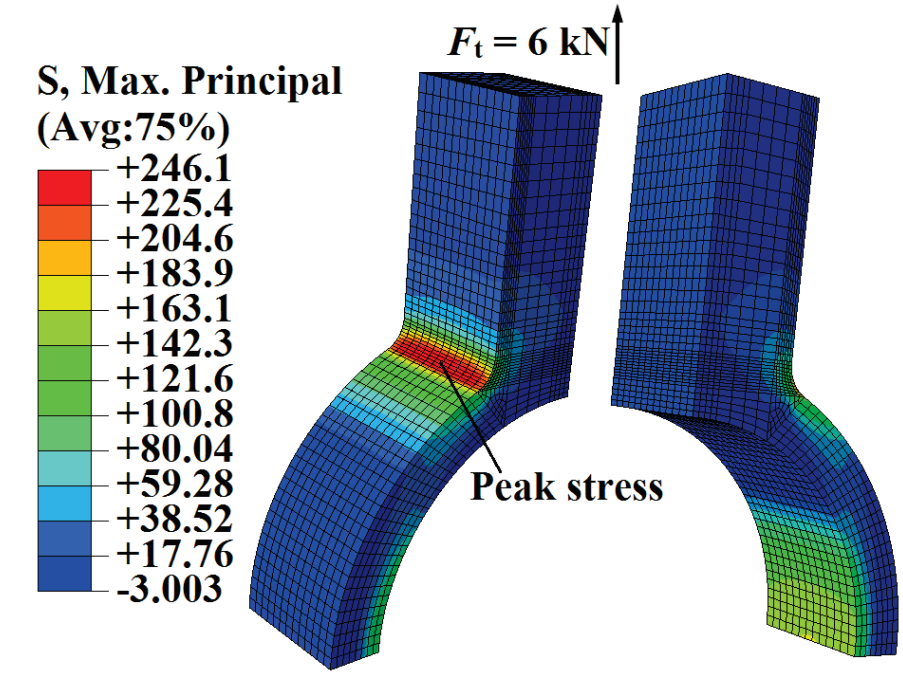

(a)

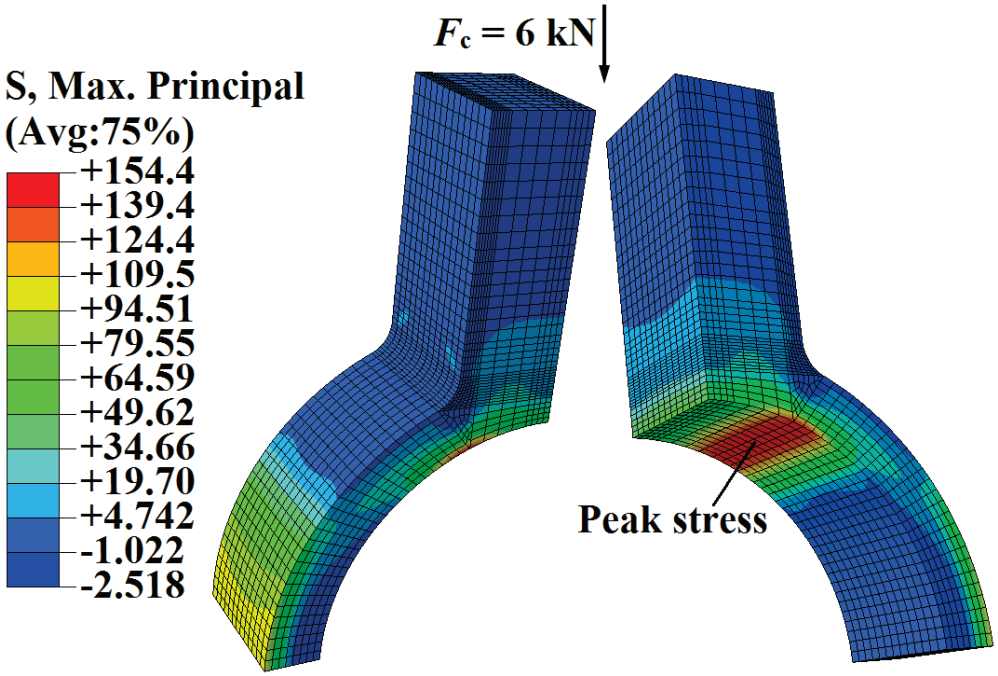

(b)

Fig. 5.3: Finite element stress field for diametral (a) tension and (b) compression.

5.3. Peak-stress method

The peak-stress was computed based on the FEA, and the fatigue limit was taken from the European Standard [16], assuming that the material used in the experiments has the same (median) plain fatigue limit σ_W under alternating stress (R = -1) as EN-GJS-600-3.

In order to consider the effect of the mean stress on the fatigue limit, a slightly modified Gerber equation [9] proposed by Zambrano et al. [2] has been used. Table 5.1 summarizes the corresponding plain fatigue limits (σ_A) at R = 0.1, the tensile and compressive fatigue limits (F_A) of the ring-shaped specimens due to the peak-stress approach and the fatigue limits for 10 % probability of failure based on Fig. 5.1.

Table 5.1: Estimated and experimentally observed (stair-case) tensile and compressive fatigue limits of ring-shaped component.

	$\delta = 1$ Goodman	$\delta = 1.62$ [2]	$\delta = 2$ Gerber	Stair-case P_f = 50 %	Stair-case P_f = 10 %
$\sigma_A(R = 0.1)$, MPa	165	193	205	-	-
F_A(tension), kN	4.0	4.7	5.0	5.7	4.5
F_A(compression), kN	6.4	7.5	8.0	7.9	7.4

5.4 Weakest link analysis

The weakest-link theory can be used in combination with the Weibull distribution to carry out non-local fatigue assessment [39]. The probability of failure of an arbitrary component (volume V) may be expressed as

$$P_{f,V} = 1 - 2^{-\left(\frac{\bar{\sigma}_a}{\sigma_{A0}}\right)^b}, \tag{5.2}$$

where σ_{A0} denotes the median fatigue limit of a uniformly stressed reference specimen of volume V_0, and

$$\bar{\sigma}_a = \left(\frac{1}{V_0} \int_V \sigma_a^b \mathrm{d}V \right)^{\frac{1}{b}} \tag{5.3}$$

the fatigue-effective (Weibull) stress amplitude.

Since even most 'plain' fatigue test specimens are not strictly uniformly stressed, the reference specimen remains fictitious and the volume V_0 arbitrary. Therefore, the median fatigue limit of the reference specimen, σ_{A0}, may be set equal to the Weibull stress amplitude of the plain fatigue test specimen used. The fatigue limit of the *component* is given by the force amplitude, at which the Weibull stress amplitude of the component equals σ_{A0}. In addition the Weibull exponents were assumed to have $b = 30$ for the machined inner surface (pulsating compression), and $b = 10$ for the as-cast outer surface (pulsating tension). The Weibull stress amplitude of the specimens have been computed by means of the weakest-link module of the in-house FEA post-processor P•FAT as described by Härkegård and Halleraker [15].

Thus the fatigue limit of the ring-shaped component under pulsating diametral compression, estimated by the weakest-link approach, was $F_A = 7.5$ kN. However for pulsating diametral tension was $F_A = 4.3$ kN.

5.5 Influence of small defects on the fatigue limit of the ring-shaped specimen

In order to assess the influence of defects on the fatigue life of the ring-shaped specimen, a small crack was inserted into the critical region as shown in Figs. 5.4a and b. The force amplitude necessary to make the crack propagate to half the specimen thickness (4 mm) in $2 \cdot 10^6$ cycles was computed.

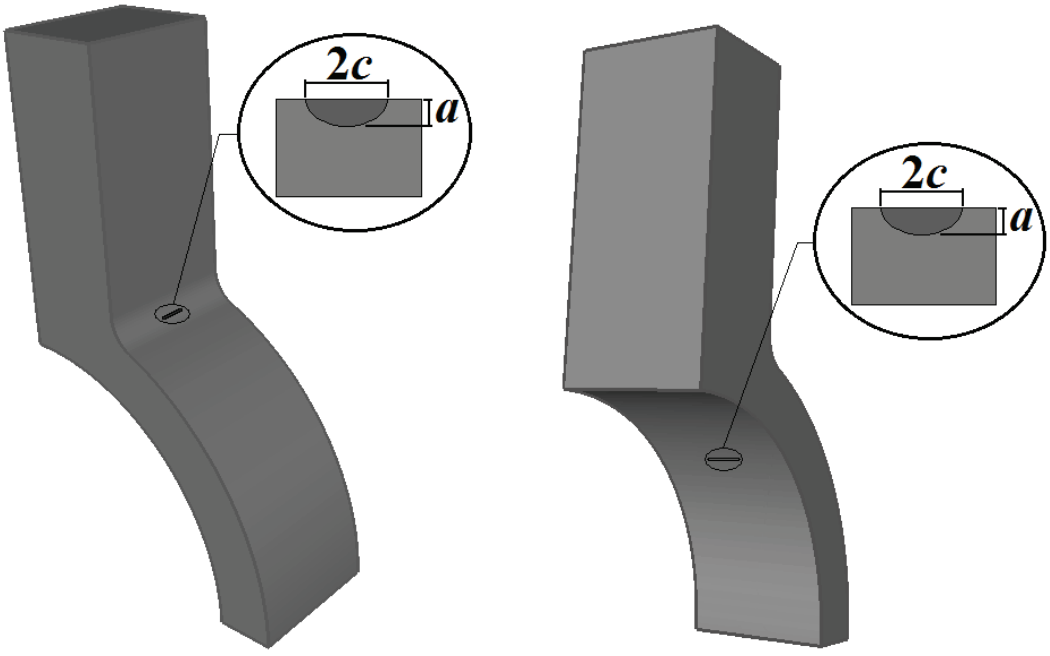

(a) (b)

Fig. 5.4: Crack-like defect for diametral (a) tension and (b) compression.

To predict accurately the fatigue life of a component containing a small crack-like defect, the fatigue crack growth law used to model the crack must take the behaviour of short cracks into account. The in-house post-processor P•FAT was used to compute the life of the component containing a small crack-like defect. This program is able to calculate ΔK from the stress field of the finite element analysis using the appropriate weight function [40]. P•FAT computes the life of the component by integrating the equation for fatigue-crack growth [20], viz.,

$$\frac{\mathrm{d}a}{\mathrm{d}N} = C\Delta K_{\mathrm{th}}^{m}\left\{\left[\left(\frac{\Delta\sigma}{\Delta\sigma_{\mathrm{A}}}\right)^{2}+\left(\frac{\Delta K}{\Delta K_{\mathrm{th}}}\right)^{2}\right]^{m/2}-1\right\}. \tag{5.4}$$

C and m are experimentally obtained constants. Eq. (5.4) predicts crack arrest when $\Delta K_{\mathrm{eq}} < \Delta K_{\mathrm{th}}$.

Different initial defect sizes were analyzed and the results are summarized in Table 5.2.

Table 5.2: Fatigue limit of the ring shaped specimen containing a small crack-like defect.

a (mm)	a/c	$\Delta\sigma_{\mathrm{A}}$ ($R = 0.1$) (MPa)	a_0 (mm)	F_{tA} (kN)	F_{cA} (kN)
1.1	0.92	386.5	0.59	3.1	4.8
0.55	0.92	386.5	0.59	3.4	5.8
0.25	0.92	386.5	0.59	4.1	7.2
0.125	0.92	386.5	0.59	4.4	7.4

CHAPTER 6

Conclusions and suggestions for further work.

The main objective of this work was achieved by means of a comprehensive investigation of the effect of notches and cracks in the fatigue limit of cast components of ductile cast iron EN-GJS-400-18-LT. To achieve the main objective the following milestone were reached:

1. Extensive investigation about the different methods available in the literature to estimate the fatigue limit of notched specimens.
2. Experimental investigation of the behavior of short cracks in the ductile cast iron EN-GJS-400-18-LT.
3. Suitable short crack growth models were developed to predict the fatigue limit of notched components based on self-arrested cracks.
4. A short crack model was used to investigate the effect of small defects in components of cast iron simulating crack-like defects. The results were compared with predictions obtained using other fatigue approaches and experimental data.

After finalizing the present investigation some suggestion come up for further work. The author consider important to investigate deeper:

1. The effect of the stress ratio on the fatigue limit in ductile cast iron.
2. The effect of the ultimate strength on ΔK_{th} in ductile cast iron.
3. The effect of the stress ratio on ΔK_{th} for $R > 0.5$ in ductile cast iron.
4. The effect of small defects randomly distributed within the components.

Bibliography

[1] Zambrano HR. Prediction of the fatigue limit of sharply notched specimens of mild steel. Submitted for publication in Proceedings of the Institution of Mechanical Engineers, Part C, Journal of Mechanical Engineering Science 2011.

[2] Zambrano HR, Härkegård G, Stärk KF. Fracture toughness and growth of short and long fatigue cracks in ductile cast iron EN-GJS-400-18-LT.Accepted for publication in Fatigue & Fract Engng Mater Struct 2011.

[3] Zambrano HR, Härkegård G. Self-arresting cracks at notches in ductile cast iron. Submited for publication in Engng Fract Mech 2011.

[4] Zambrano HR, Härkegård G. Fatigue testing and modeling of a ring-shaped specimen of ductile cast iron. Submitted for publication in Eng Fail Anal 2011.

[5] Leis BN, Topper TH. Cyclic deformation and fatigue analysis for notched components. Nucl Engng Design 1974; p. 370-83.

[6] Frost NE. A relation between the critical alternating propagation stress and crack length for mild steel. Proc Instn Mech Engrs 1959; vol. 173, p. 811-27.

[7] Peterson RE. Notch sensitivity. In: Sines G, Waisman JL, editors. Metal fatigue. New York: MacGraw-Hill, 1959.

[8] Neuber H. Kerbspannungslehre. Theory of notches [Edwards JW, Eng Trans]. Ann Arbor MI: Springer-Verlag; 1946.

[9] Dowling NE. Mechanical behavior of materials: engineering methods for deformation fracture and fatigue. 3rd ed. Prentice Hall; 2007.

[10] Siebel E, Stieler M. Ungleichförmige Spannugsverteilung bei schwingender Beanspruchung. *VDI-Zeitschrift* 97 1955; p. 121-26.

[11] Rechnerischer Festigkeitsnachweis für Maschinenbauteile aus Stahl, Eisenguss und Aluminiumwerkstoffen, FKM-Richtlinie, 5. erweiterte Auflage. VDMA; 2003. p. 108f [English edition: Analytical strength assessment. 5th ed. VDMA Verlag. ISBN: 3-8163-0425-7].

[12] Taylor D. The theory of critical distances: a new perspective in fracture mechanics. Elsevier; 2007.

[13] El Haddad M H, Topper TH, Smith KN. Prediction of non-propagating cracks. Eng Fract Mech 1979; 11:573-84.

[14] Smith RA, Miller KJ. Prediction of fatigue regimes in notched specimens. Int. J. Mech. Sci 1978; 20(4):201-06.

[15] Härkegård G, Halleraker G. Assessment of methods for prediction of notch and size effects at the fatigue limit based on test data by Böhm and Magin. Int J Fatigue 2010; 32 1701-09.

[16] European Standard EN 1563:1997, Founding – Spheroidal graphite cast iron, CEN, June 1997.

[17] Verdu C, Adrien J, Buffière JY. Three-dimensional shape of the early stages of fatigue cracks nucleated in nodular cast iron. Mater Sci Eng A 2007;483-484:402-05.

[18] Murakami Y. Metal fatigue: effect of small defects and non metallic inclusions. Elsevier; 2002. [ISBN: 0-08-044064-9].

[19] Nadot Y, Mendez J, Ranganathan N. Influence of casting defects on the fatigue limit of nodular cast iron. Int J Fatigue 2003;26:311-19.

[20] Fjeldstad A, Wormsen A, Härkegård G. Simulation of fatigue crack in components with random defects. Engng Fract Mech 2007;75:1184-1203.

[21] Beretta S, Blarasin A, Endo M, Giunti T, Murakami Y. Defect tolerance design for automotive components. Int J Fatigue 1997; 19(4):319-33.

[22] Skallerud B, Iveland T, Härkegård G. Fatigue life assessment of aluminium alloys with casting defects. Engng Fract Mech 1993; 44(6):857-74.

[23] Hübner P, Schlosser H, Pusch G, Biermann H. Load history effects in ductile cast iron for wind turbine components. Int J Fatigue 2007; 29:1788-1796.

[24] Tokaji K, Ogawa T, Shamoto K. Fatigue crack propagation in spherical graphite cast iron with different microstructures. Int J Fatigue 1994;16(5):344-50.

[25] Cavallini M, Bartolomeo Di O, Iacoviello F. Fatigue crack propagation damaging micromechanisms in ductile cast irons. Engng Fract Mech 2007; 75:694-704.

[26] Shirani M, Härkegård G. Fatigue crack growth simulation in components with random defects. J ASTM Int 2009; 6(9).

[27] ASTM E1820-09. Standard test method for measurement of fracture toughness. West Conshohocken. Annual book of ASTM standards; 2010.

[28] Denk J, Amhof S. Determination of the high cycle fatigue strength with a load-increasing single-specimen technique. In: Lütjering G, Nowack H, editors. FATIGUE 96, Proceedings of the Sixth International Fatigue Congress held in Berlin, Germany, 6–10 May 1996. Sheffield: EMAS Publishing; 1996 (ISBN 0 08 0422683).

[29] Mann T, Härkegård G, Stärk K. Short fatigue crack growth in aluminium alloy 6082-T6. Int J Fatigue 2007;29:1820-26.

[30] Klesnil M, Lukáš P. Influence of strength and stress history on growth and stabilisation of fatigue cracks. Engng Fract Mech 1972; 4(1): 77–92.

[31] Mann T. The influence of mean stress on fatigue crack propagation in aluminium alloys. Int J Fatigue 2006; 29: 1393-1401.

[32] Härkegård, G. An effective stress intensity factor and the determination of the notched fatigue limit, Fatigue Thresholds, Vol. II, Eds. J. Bäcklund et al., EMAS, Warley, UK, 1981; 867-879.

[33] Taylor D, Hughes M, Allen D. Notch fatigue behaviour in cast irons explained using a fracture mechanics approach. Int J Fatigue 1996; 18(7): 439-45.

[34] Fjeldstad A. Modelling of fatigue crack growth at notches and other stress raisers. Doctoral Theses at NTNU 2007; 231.

[35] Liu Y, Mahadevan S. Fatigue limit prediction of notched components using short crack growth theory and asymptotic interpolation method. Engng Fract Mech 2008; 76: 2317-2331.

[36] Yates JR, Brown MW. Prediction of the length of non-propagating cracks. Fatigue Fract Engng Mater Struct 1987; 10 (3): 187-201.

[37] Palmer KB, Gilbert GNJ. BCIRA Research Report 361. Journal of Research and Development 1953; 5(1): 2-14.

[38] Shirani M. Probabilistic and defect tolerant fatigue assessment of wind turbine castings. Doctoral theses at NTNU, 2011:153

[39] Wormsen A, Sjödin B, Härkegård G, Fjeldstad A. Non-local stress approach for fatigue assessment based on weakest-link theory and statistics of extremes. Fatigue Fract Engng Mater Struct 2007;30:1214-27.

[40] Wormsen A, Fjeldstad A, Härkegård G. A post-processor for fatigue crack growth analysis based on a finite element stress field. Computer Methods in Applied Mechanics and Engineering 2007; 197(6-8): 834-845.

Paper 1

Is not included due to copyright

Paper 2

Is not included due to copyright

Paper 3

Is not included due to copyright

Paper 4

Is not included due to copyright